Construction and Building Materials 504 (2025) 144603

Contents lists available at ScienceDirect

Construction and Building Materials

journal homepage: www.elsevier.com/locate/conbuildmat

Effects of recycled concrete powder on shrinkage, mechanical, and thermal behaviours of multi-walled carbon nanotubes-reinforced engineered geopolymer composites

Yuekai Xie [a,b,*], Aziz Ahmed [a], Y.X. Zhang [c]

[a] School of Civil, Mining, Environmental and Architectural Engineering, University of Wollongong, Wollongong, NSW 2522, Australia
[b] School of Engineering and Technology, University of New South Wales, Canberra, ACT 2600, Australia
[c] School of Mechanical and Mechatronic Engineering, Faculty of Engineering and Information Technology, University of Technology Sydney, 81 Broadway, Ultimo, NSW 2007, Australia

ARTICLE INFO

Keywords:
Autogenous shrinkage
Drying shrinkage
Engineered geopolymer composite
Multi-walled carbon nanotube
Recycled concrete powder
Thermal resistance

ABSTRACT

Although multi-walled carbon nanotubes (MWCNTs) can enhance the performance of engineered geopolymer composite (EGC), the related high costs and carbon emissions remain significant challenges. This study explored the feasibility of incorporating construction waste-derived recycled concrete powders (RCPs) as fine aggregates in EGC reinforced by polyethylene (PE) fibres or hybrid MWCNTs and PE fibres. The investigated properties included drying and autogenous shrinkage, compressive and tensile performance, and thermal resistance up to 600 °C, together with cost-benefit and carbon footprint analyses. The results demonstrate that replacing natural aggregates with 75 % RCPs in MWCNT-EGC contributes to improved shrinkage, mechanical, thermal, economic, and environmental performance, while only 25 % RCPs in EGC is favourable for the compressive strength. After thermal exposure to 140 °C, MWCNT-EGC with 75 % RCPs exhibits improved tensile strength (9.49 MPa) and comparable strain capacity (9.98 %) to those at ambient temperature. After thermal exposure to 600 °C, the residual compressive strength of MWCNT-EGC with 75 % RCPs maintains 80.4 MPa, 58.2 % higher than the control group. The cost-benefit analysis and carbon footprint assessment indicate that introducing 75 % RCPs reduces costs and associated carbon emissions to achieve a unit strength than the conventional EGC with varying proportions of RCPs but without MWCNTs. These findings suggest that incorporating 75 % RCPs as fine aggregates is a financially viable and environmentally sustainable solution for MWCNT-EGC production.

1. Introduction

Engineered cementitious composite is a high-performance fibre-reinforced material with high tensile ductility over 2 % and excellent multiple micro-cracking capacity [1]. The unique strain-hardening behaviour of ECC makes it promising for infrastructures subjected to seismic, fatigue, and impact loading. ECC is typically prepared by cement, fine aggregates, fibres, superplasticisers, water, and/or supplementary cementitious materials (SCMs) [2]. However, the high energy consumptions and carbon emissions with cement binder production raises significant environmental concerns [3,4]. Although partial replacement of cement by SCMs derived from industrial byproducts or waste materials like recycled ceramic powder mitigates environmental concerns, the overall carbon emissions of cementitious composites remain high because of low aggregate-to-binder ratios [5,6]. One alternative to conventional cement binder is geopolymer, which is produced by alkaline-activation of aluminosilicate-rich industrial byproducts (precursor) such as fly ash (FA), silica fume (SF), and ground granulated blast-furnace slag (GGBFS) [7–9]. Compared to cement binder, the typical carbon emissions from geopolymer are 44–64 % lower [10]. Therefore, by replacing cement with geopolymer, the engineered geopolymer composite (EGC) has been developed as an alternative to ECC. EGC is typically prepared by precursors, fine aggregates, fibres, water, and/or superplasticizers [11]. Similar to ECC, engineered geopolymer composite (EGC) is a fibre-reinforced material with ultra-high ductility and micro-crack width control capacity, which demonstrates comparable or improved mechanical properties and thermal resistance as ECC but with a lower carbon footprint [12].

* Corresponding author at: School of Civil, Mining, Environmental and Architectural Engineering, University of Wollongong, Wollongong, NSW 2522, Australia.
E-mail address: yuekaix@uow.edu.au (Y. Xie).

https://doi.org/10.1016/j.conbuildmat.2025.144603
Received 13 August 2025; Received in revised form 18 November 2025; Accepted 20 November 2025
Available online 21 November 2025

While geopolymer-based materials provide a promising solution to sustainable materials, their performance could be further enhanced by various additives. Nanomaterials, such as graphene [13], nano-silica [14,15], cellulose nanocrystals [16], and multi-walled carbon nanotubes (MWCNTs) [17], have been incorporated into geopolymer-based materials to improve their mechanical properties. Among these, MWCNTs provide excellent advantages for EGC [18], and the ultra-high tensile strength and modulus and aspect ratios of the MWCNTs are favourable for the crack bridging capacity and tensile performance [19]. In addition to mechanical behaviours, introducing MWCNTs mitigates autogenous and drying shrinkage of EGC due to filler and bridging effects [20]. The formed micro-cracks are bridged by MWCNTs, inhibiting the development of micro-cracks. The structural compactness is improved as micro-voids are filled by MWCNTs [21]. Besides, the ultra-fine sizes of MWCNTs are beneficial to the prevention of initiation, propagation, and expansion of micro-cracks under the elevated temperatures [12]. The MWCNTs maintained structural stability before 620 °C, and the residual compressive strength of MWCNT-reinforced engineered geopolymer composite (MWCNT-EGC) remained 78.1 % and 58.0 % at the elevated temperatures of 600 and 800 °C, respectively, significantly higher than conventional EGC [12]. However, the high unit cost and carbon emissions associated with MWCNTs potentially raise economic and environmental concerns [22]. The associated costs and carbon emissions to achieve unit strength of EGC with MWCNTs could be significantly higher than pure EGC [23].

In addition to nanomaterials, recycled concrete powders (RCPs) have been regarded as sustainable aggregates in geopolymer-based materials. The RCPs are recycled materials typically prepared by crushing and grinding recycled concrete aggregates (RCAs) from construction and demolition wastes (CDW). Globally, the annual production of CDW reaches 3 billion tons [24]. Instead of disposal in landfills, incorporating RCAs and RCPs in construction materials such as EGC presents a significant opportunity for valorisation, offering a dual sustainability benefit by diverting a major waste stream from landfills while simultaneously reducing the consumption of virgin materials [25,26]. While the introduction of RCAs as coarse aggregates has demonstrated potential in shrinkage mitigation due to internal curing effects [27], their large sizes limit the application in EGC, where fine aggregates are used. Therefore, most of the previous studies focused on the mechanical properties of EGC with partial to full proportion of GGBFS replaced by RCPs, i.e., application of RCPs as a precursor [8,26,28]. Although the results in these studies demonstrated that the introduction of RCPs reduced the overall carbon footprint from raw materials, the abundant calcite and inactive quartz with limited reactivity in RCPs inhibited the geopolymerisation reactions, leading to reduced mechanical properties such as compressive strength.

On the other hand, if used as fine aggregates, the presence of portlandite in RCPs is potentially beneficial for geopolymerisation reactions, forming additional C(A)SH gels [29]. Xie et al. [30] investigated the mechanical behaviours and thermal stability of EGC with varying RCPs' proportions as aggregates and found that EGC with 75 % RCPs exhibited higher mechanical properties and residual strength at 400 and 600 °C than that without RCPs. The strength increments result from enhanced gel productions and filler effects of RCPs. In addition, the lightweight nature of RCPs could contribute to a lower density of EGC, i.e., the quantity of virgin material consumptions can be reduced, leading to decreased costs and emissions [30]. The unit cost of carbon emission to achieve unit strength of MWCNT-EGC can be decreased. Therefore, the incorporation of RCPs in MWCNT-EGC is expected to produce a more sustainable EGC with reduced shrinkage, enhanced mechanical properties, and improved thermal resistance compared to that containing only virgin aggregates. However, the effects of using RCPs as fine aggregates on shrinkage, mechanical properties, and thermal resistance of MWCNT-EGC matrix have not been systematically evaluated.

This paper focused on the development of an MWCNT-EGC with mitigated shrinkage, improved mechanical properties (e.g., compressive strength over 120 MPa and tensile strain capacity over 9 %), and enhanced thermal stability by replacing the fine aggregates with RCPs. The autogenous and drying shrinkage, compressive and tensile behaviours, and those after thermal exposures were investigated. The variation in degrees of geopolymerisation reactions due to RCPs was evaluated by X-ray diffraction (XRD) and thermogravimetric analysis-derivative thermogravimetry (TGA). The costs and emissions associated with virgin materials were evaluated based on the quantity used for unit MWCNT-EGC production and relevant costs/carbon emissions. To demonstrate the excellence of MWCNT-EGC, additional EGC groups with varying RCPs' proportions were prepared. In addition to improved shrinkage (autogenous shrinkage from 5683 to 4859 με and drying shrinkage from 9497 to 7414 με), mechanical performance (compressive strength from 89.6 to 120.8 MPa, tensile strength from 6.27 to 8.20 MPa, and strain capacity from 8.46 % to 9.96 %), and thermal durability (strength retention factor from 56.7 % to 66.5 % after 600 °C), MWCNT-EGC with 75 % RCPs also exhibited lower cost and embodied carbon (i.e., reduced cost and carbon footprint to achieve a unit strength) than the conventional EGC with varying RCPs' proportions, demonstrating that replacing fine aggregates with RCPs could offset the high unit cost and carbon emissions associated with MWCNTs.

2. Materials and methodology

2.1. Materials

The precursor for MWCNT-EGC comprised 20 % FA and 80 % GGBFS by mass. The high proportion of GGBFS was utilised to achieve high compressive and tensile strength of EGC [31]. For example, rising GGBFS contents from 20 % to 80 % increased compressive and tensile strength of EGC from 50.8 to 89.6 MPa and 4.23–6.23 MPa, respectively [32]. The FA and GGBFS were from local coal combustion and steel manufacturing plants, respectively. The composition and scanning electron microscope (SEM) images of FA and GGBFS are illustrated in Table 1 and Fig. 1(a, b), respectively. Both FA and GGBFS are abundant in aluminosilicate contents, which are favourable for geopolymerisation reactions [33].

The 8 M sodium hydroxide (SH) and sodium silicate solutions (SS) were adopted as alkaline activators. The higher concentration of SH decreased the strength of the geopolymer and led to increased carbon footprint, as indicated by Song et al. [34]. The mass fractions of Na_2O, SiO_2, and H_2O in SS were 14.7 %, 29.4 %, and 55.9 %, respectively. The mass ratio between SS and SH was 2.5, which was favourable for the strength development of geopolymer [35].

Quartz sand (QS) with sizes smaller than 300 μm was used as fine aggregate. The PE fibres were employed because of their exceptional tensile properties and micro-crack bridging capacity. The strain-hardening behaviours of EGCs could be improved by controlled micro-crack propagation and reduced strain localisation provided by PE fibres [8]. The length, diameter, density, tensile strength, and elastic modulus of polyethylene (PE) fibres were 12 mm, 0.024 mm, 0.97 g/cm^3, 3 GPa, and 116 GPa, respectively. The diameters of MWCNTs ranged from 50 to 100 nm (Fig. 1(d)), with tensile strength and elastic modulus of 30 and 900 GPa, respectively. To improve the flowability of MWCNT-EGC, the polycarboxylate-based superplasticiser (SP) was incorporated.

The RCPs were prepared by grinding fine RCAs (smaller than 4.75 mm) from the Mugga Lane Resource Management Centre, Canberra. These RCAs were mainly from demolished infrastructures with long service life. Before grinding, all samples were sorted based on particles finer than 75 μm, 75–300 μm, 300 μm to 1.18 mm, 1.18 mm to 4.75 mm, and then remixed according to the particle size distribution of all batches. The grinding process (300 rpm for 3 min) was adopted for each batch, which facilitated the reactivity of RCPs via reducing particle sizes and increasing surface areas, which increased the contact between the particles and alkaline activators [36]. After grinding, the samples

Table 1
Compositions of FA, GGBFS, and RCPs (wt%).

Element	Na_2O	MgO	Al_2O_3	SiO_2	SO_3	K_2O	CaO	Fe_2O_3	Loss on ignition
FA	0.41	0.59	19.55	69.32	0.09	1.28	2.68	4.24	1.84
GGBFS	0.26	5.08	12.25	34.69	1.61	0.35	44.32	1.19	0.25
RCP	1.15	2.58	7.15	61.54	0.53	1.00	16.48	2.75	6.82

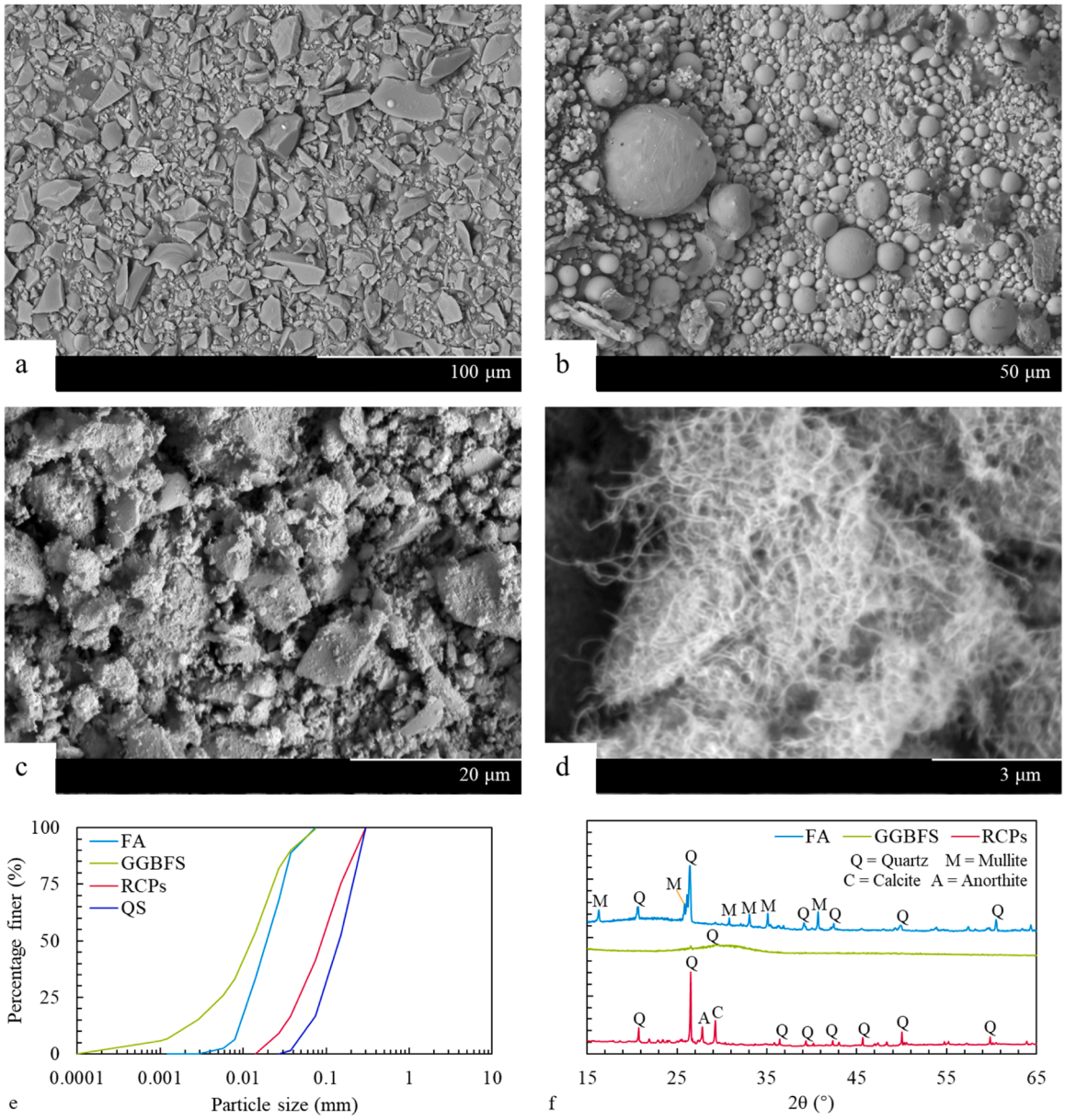

Fig. 1. Properties of raw materials: (a). SEM of FA, (b). SEM of GGBFS, (c). SEM of RCPs, (d). SEM of MWCNTs, (e). Particle size distribution of FA, GGBFS, and RCPs, (f). XRD of FA, GGBFS, and RCPs.

from all batches were screened by a 300 μm mesh and characterised as finer than 75 μm, 75–150 μm, and 150 μm to 300 μm. These RCPs with different particle sizes were remixed again based on the average particle size distribution to ensure similar particle sizes and reactivity of RCPs used for mixing. The SEM image of RCPs is presented in Fig. 1(c). De Rossi et al. [37] suggested that fine-sized RCPs were favourable for the filler effect, promoting strength development from the investigation of the mechanical properties of geopolymer mortar with varying particle sizes of RCPs. Therefore, RCPs with finer grain sizes than QS were adopted (Fig. 1(e)). The water absorptions of QS and RCPs are 2.6 % and 8.2 %, respectively, indicating RCPs have more permeable voids than QS. The XRD of FA, GGBFS, and RCPs are presented in Fig. 1(f). In addition to quartz, major phases of RCPs were calcite and anorthite. The specific gravity of FA, GGBFS, and QS was 2.42, 2.84, 2.60, and 2.46, respectively.

2.2. Sample preparation

Based on the preliminary results shown in Table 2, Table 3 lists the mix designs for MWCNT-EGC of varying RCPs' proportions. The

Table 2
Mechanical properties of MWCNT-EGC with varying MWCNTs' contents (Xie [23]).

MWCNT content	Compressive strength (MPa)	Tensile strength (MPa)	Strain capacity (%)
0.0 %	89.6 ± 1.5	6.27 ± 0.26	8.46 ± 0.55
0.1 %	94.7 ± 4.2	6.64 ± 0.25	8.86 ± 0.24
0.2 %	100.4 ± 2.2	7.34 ± 0.20	9.19 ± 0.22
0.3 %	103.0 ± 3.3	7.62 ± 0.12	8.91 ± 0.40
0.4 %	104.3 ± 3.3	7.69 ± 0.20	8.71 ± 0.23

replacement rates of QS by RCPs were 25 %, 50 %, 75 %, and 100 %, as adopted in previous studies [29,30]. The PE fibres with 2 % volumetric fraction were favourable for the tensile behaviour of EGC, as suggested in a previous study [30]. To validate the effects of RCPs on EGC, 5 mix proportions with varying RCPs' proportions and 0 % MWCNTs were set up for preliminary investigation. The results indicated that the incorporation of 25 % RCPs contributed to enhanced compressive strength, and tensile performance (i.e., tensile strength and strain capacity) degraded with increasing RCPs' contents.

Xie [23] suggested that 0.2 % MWCNTs contributed to the highest strain capacity (summarised in Table 2) and thermal stability of MWCNT-EGC. Although the further inclusion of MWCNTs still slightly improved the mechanical performance ($p > 0.05$), the relevant cost to produce MWCNT-EGC increased significantly. Therefore, a constant MWCNTs' dosage of 0.2 % was adopted. To achieve sufficient dispersion, MWCNTs were added to the alkaline activators, followed by mixing for 15 min at 1500 rpm. The solution was then subjected to sonication for 30 min, with a corresponding amplitude of 50 %, as adopted in previous studies [38]. To ensure adequate dispersion of MWCNTs, 40 mL samples were collected from the upper, middle, and lower layers of the solution, with triplicate samples in each layer. The collected samples were dried at 105 ± 5 °C until constant mass. The variations between the highest and lowest mass were within 7.76 %, indicating adequate dispersion.

To prevent absorption of alkaline activators by aggregates, additional water was mixed with RCPs and QS (Table 3). The alkaline activator-MWCNT mixture (or only alkaline activator) was mixed with the precursor for 2 min, followed by the addition of the water-aggregate mixture and SP, and 2 min of blending. Finally, PE fibres were introduced and blended for 3 min. The fresh mixture was cast in 50 mm cube moulds, 160 × 40 × 40 mm prismed moulds, 366 × 80 × 20 mm dog-bone moulds, with a narrowed gauge section of 100 × 30 × 20 mm (Fig. 2(a)), and corrugated pipes (Section 2.3.1). The cubic, prismatic, dog-bone, and corrugated-pipe specimens were used for compressive strength (unconfined), drying shrinkage, tensile behaviour, and autogenous shrinkage testing, respectively. The specimens were cured under 23 ± 2 °C and a relative humidity of 60 ± 5 %. After 28-day curing, the permeable porosity was determined according to ASTM C642 [39] with 3 prism samples for each mix proportion.

2.3. Testing procedures

2.3.1. Shrinkage measurement

The autogenous shrinkage was determined with the corrugated pipes, whose diameter and length were 25 and 420 mm, respectively [40]. The fresh paste was cast into the pipes and vibrated to eliminate air voids. After the final setting time (30 min), the initial length was measured by a displacement gauge. The variation in length of the specimens was then recorded with time. For the drying shrinkage, the prism samples were demoulded after 30 min of casting, as consistent with the autogenous shrinkage [41]. The changes in mass and length were measured accordingly. The total duration of the shrinkage measurement was 90 days. For both autogenous and drying shrinkage, the values at various durations could be determined using Eq. (1).

$$\varepsilon_t = \frac{L_t - L_0}{L_0} \times 10^6 \quad (1)$$

Where ε_t = shrinkage of the specimen (με),

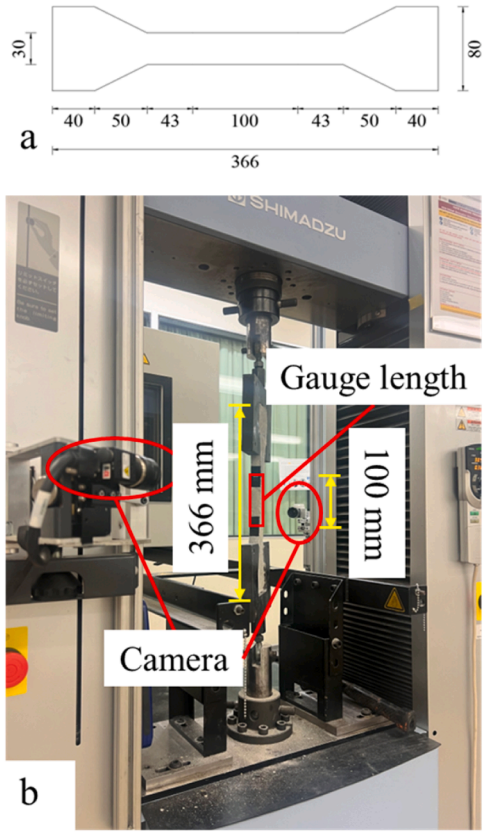

Fig. 2. Diagram for tensile experiments: (a). Dimensions of dog-bone samples, (b). Experimental setup.

Table 3
Mix proportion designs of MWCNT-EGC with varying RCPs' contents (kg/m^3).

Mix	GGBFS	FA	QS	RCPs	SH	SS	Water	SP	PE fibres	MWCNTs
C0R0	840	210	630	0	126	315	98	10.5	19.4	0.00
C0R25	835	209	470	157	125	313	98	10.4	19.4	0.00
C0R50	830	208	311	311	125	311	97	10.4	19.4	0.00
C0R75	825	206	155	464	124	309	96	10.3	19.4	0.00
C0R100	820	205	0	615	123	308	96	10.3	19.4	0.00
C2R0	840	210	630	0	126	315	98	10.5	19.4	2.10
C2R25	835	209	470	157	125	313	98	10.4	19.4	2.09
C2R50	830	208	311	311	125	311	97	10.4	19.4	2.08
C2R75	825	206	155	464	124	309	96	10.3	19.4	2.06
C2R100	820	205	0	615	123	308	96	10.3	19.4	2.05

L_0 = initial length of the specimens (mm),
L_t = length of the specimens after duration t (mm).

2.3.2. Mechanical testing

The (unconfined) compressive and tensile behaviours of EGC and MWCNT-EGC were measured according to ASTM C109/109 M [42] and JSCE standards [43], with corresponding rates of 0.33 MPa/s and 0.1 mm/min, respectively. The cube samples cured for 7, 14, and 28 days were used for compression testing, and the dog-bone specimens cured for 28 days were adopted for tensile testing, with a gauge length of 100 mm Fig. 2(b). Triplicate samples were used for each test.

2.3.3. Thermal stability

To investigate the thermal stability of MWCNT-EGC with varying RCPs' proportions, the dog-bone samples were subjected to the heating rates of 2, 4, and 6 °C/min for 20 min to reach 60, 100, and 140 °C, respectively. The tensile behaviour of cooled samples was measured following the same procedures as Section 2.3.2. The tensile performance of EGC (except the control group) was not studied as the incorporation of RCPs decreased the tensile strength and strain capacity. In addition to these temperature ranges, the cubic specimens of EGC and MWCNT-EGC were heated at 19 and 29 °C/min for 20 min to 400 and 600 °C, respectively. The compression processes of cooled samples were the same as those mentioned in Section 2.3.2. Same as that mentioned in Section 2.3.2, triplicate samples were adopted for each test.

2.3.4. Microstructural analyses

To determine the influence of RCPs on geopolymer products of EGC and MWCNT-EGC, the microstructural analysis was conducted, including XRD and TGA-DTG. The fragments after compressive testing were soaked in acetone for 48 h, air-dried at 60 °C for 24 h, milled and sieved by a 300 μm mesh. The XRD analyses were conducted with 2θ varying from 15° to 65°. A scanning speed of 2°/min was adopted. The TGA-DTG tests were conducted with the heating rate of 10 °C/min. The corresponding temperature ranges were between 50 and 750 °C.

2.4. Economic and environmental assessment

The feasibility of RCPs for MWCNT-EGC production is relevant to the production costs and carbon emissions. The market price of GGBFS, FA, QS, RCPs, SH, SS, SP, and PE fibres in Australia can be found in Xie et al. [30], while that of MWCNTs is based on Xie [23]. The embodied carbon of raw materials was based on the life cycle assessment performed in the literature, representing cradle-to-gate results, i.e., extraction, processing, fuel combustion, and transportation [8,32,44,45]. The values of solutions are correlated with the corresponding concentrations. The embodied carbon of RCPs is higher than typical RCAs due to additional grinding process [8]. It should also be highlighted that the carbon emission from MWCNT is based on the industrial scale, as determined by Teah et al. [22]. The sonication process was assumed to be conducted with an industrial device with capacity of 500 L and power of 4 kW. The relevant cost is 0.26 AUD/kWh. The carbon footprint of electricity from coal combustion was 1 kg CO_2/kWh, based on the median value of 164 studies summarised in Whitaker et al. [46]. The estimation of the unit costs (Eq. (2)) and carbon footprints (Eq. (3)) was based on the values listed in Table 4 and mix proportions shown in Table 3.

$$Total\ cost = \sum_{i=1}^{n} m_i C_i \tag{2}$$

Where m_i = mass of material i in the mix (kg/m^3),
C_i = cost of material i (AUD/kg).

$$Total\ carbon\ footprint = \sum_{i=1}^{n} m_i EC_i \tag{3}$$

Table 4
Market price and carbon footprint of raw materials for MWCNT-EGC production.

Material	Price (AUD/kg)	Carbon footprints (kg CO_2/kg)
GGBFS	0.16	0.070
FA	0.12	0.010
QS	0.03	0.024
RCPs	0.02	0.028
SH	0.21	0.358
SS	0.60	0.289
SP	1.80	0.584
PE fibres	5.00	2.00
MWCNTs	90.0	20.0

Where EC_i = embodied carbon of material i (kg CO_2/kg).

3. Results and discussion

3.1. Microstructural analysis

3.1.1. XRD

The XRD patterns of EGC and MWCNT-EGC with varying RCPs' dosages are presented in Fig. 3(a) and (b), respectively. The inclusion of RCPs causes an additional phase of anorthite, as included in the aggregates of RCPs. An increase in RCPs' contents corresponded to a higher intensity of the peak observed at 27.9°. The intensity of quartz and mullite decreases with increasing RCPs replacement rates. In addition to those phases, Fig. 3(c) and (d) illustrate the results of the highlighted (orange) areas in Fig. 3(a) and (b), respectively. The hump between 28° and 32° demonstrates the productions of C(A)SH. The calcite is mainly from RCPs, and the relevant intensity of the peak increases with RCPs' proportions. The overall intensity and area of the hump from 28° to 32° exhibits improvement with RCPs' dosages from 0 % to 25 % for EGC and 0–75 % for MWCNT-EGC, illustrating potential enhanced reactions and gel formations. For EGC, over 25 % RCPs are adverse for the geopolymerisation reactions. For MWCNT-EGC, the complete replacement inhibits the geopolymerisation processes and gel productions compared to 75 % RCPs. However, XRD results alone do not provide quantitative results, the detailed gel productions will be further analysed by TGA-DTG in Section 3.1.2.

3.1.2. TGA-DTG

Fig. 4(a) and (b) present the TGA of EGC and MWCNT-EGC with varying RCPs' proportions, with corresponding DTG illustrated in Fig. 4 (c) and (d), respectively. The RCPs exhibit a small DTG peak centred at 107 °C, indicating the removal of bound water. Another DTG peak is observed between 392 and 476 °C due to dehydroxylation of portlandite [47]. However, portlandite-relevant peaks are not clearly determined in the XRD of RCPs (Fig. 1(b)), suggesting portlandite is poorly crystallised. The decomposition of calcite in RCPs is reflected by the sharp DTG peak between 635 and 728 °C [48]. Similarly, EGC and MWCNT-EGC demonstrate significant DTG peaks from 50 to 220 °C because of the exclusion of free and bound water [23]. The hump-like DTG from 220 to 580 °C was caused by dehydroxylation of C(A)SH gels [30,32]. No obvious peak for dehydroxylation of portlandite is determined for C0R0, C0R25, C2R0, C2R25, C2R50, and C2R75, while there is a small portlandite-related peak in C0R50, C0R75, C0R100, and C2R100, suggesting excessive portlandite remained in the matrix. The DTG peak from 575 to 700 °C is caused by the degradation of calcite [30,32].

The mass changes during the discussed temperature ranges are demonstrated in Table 5. The higher mass changes from 50 to 220 °C are caused by the increased water absorption capacity of RCPs and promoted gel formations. The reduction in the mass loss with RCPs increasing from 25 % to 100 % in EGC and from 75 % to 100 % in MWCNT-EGC suggests inhibited reactions associated with excessive RCPs, as consistent with XRD. The mass loss during the second stage (220–580 °C) is caused by dehydroxylation of C(A)SH gels and

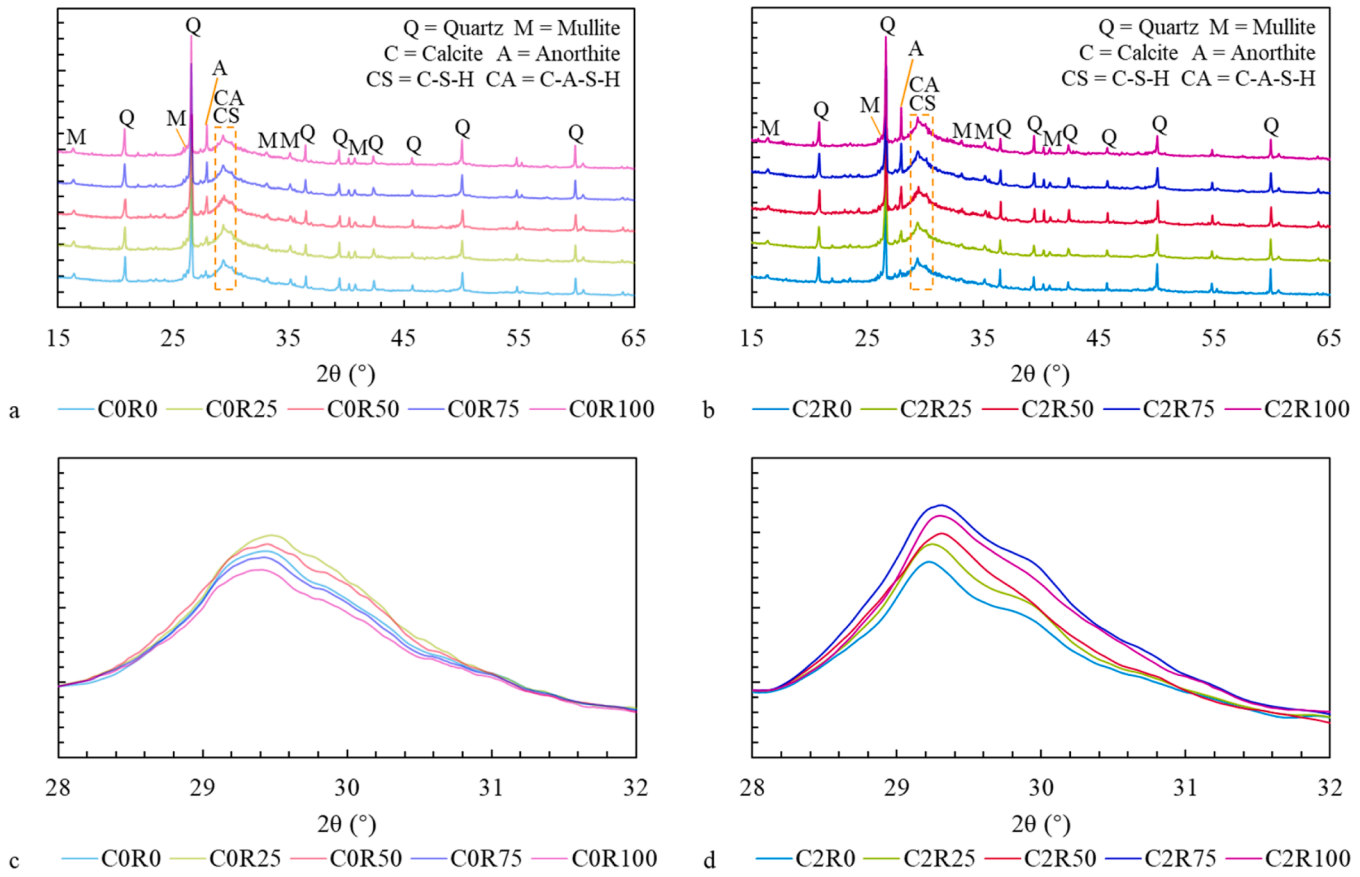

Fig. 3. Effects of RCPs on XRD: (a). XRD of EGC, (b). XRD of MWCNT-EGC, (c). Highlighted (orange) hump areas of EGC, (d). Highlighted (orange) hump areas of MWCNT-EGC.

portlandite, particularly when RCPs are incorporated. The relatively small increments with RCPs' proportions from 0 % to 25 % in EGC and 0–75 % in MWCNT-EGC suggest that portlandite was involved in the chemical reactions during alkali-activation. The increment with each additional 25 % RCPs replacement rate is smaller than the expected amount if portlandite is not reacted. For example, RCPs constitute around 7 %, 14 %, and 21 % of the total mass of C2R25 (or C0R25), C2R50, and C2R75, respectively. The additional mass loss will be 0.56 %, 1.12 %, and 1.68 % if portlandite remains unreacted, i.e., mass loss increases by 0.56 % with every 25 % RCPs. However, the actual increase with 25 %, 50 %, and 75 % RCPs' replacement in MWCNT-EGC is 0.18 %, 0.35 %, and 0.59 %, indicating that significant fractions of portlandite have been transformed into C(A)SH gels, resulting in less mass change than pure portlandite. When RCPs' replacement rates increase to 100 %, the increment in mass change (0.60 %) compared to 75 % RCPs exceeds 0.56 %. The relatively large mass loss suggests that incorporating 100 % RCPs inhibits geopolymerisation reactions compared to adding 75 % RCPs. Similarly, incorporating 25 % RCPs in EGC is favourable for gel production, whereas further inclusion of RCPs inhibits the reactions. The stable increment in the mass loss from 580 to 750 °C with increasing RCPs' dosages from 0 to 75 % demonstrates that part of the calcite participates in the chemical reactions. The substantial increment in mass loss from C2R75 to C2R100 illustrates inhibited reactions associated with excessive RCPs. A similar trend can be found for EGC with 25 % RCPs and 50–100 % RCPs.

The XRD and TGA-DTG demonstrate a consistent trend regarding the effects of RCPs. The replacement of QS with 25 % RCPs in EGC and up to 75 % RCPs in MWCNT-EGC facilitates the productions of C(A)SH gels, which are favourable for strength development. The improved gel productions are relevant to autogenous curing of RCPs, nucleation sites from calcite and MWCNTs [23], and additional calcium sources from portlandite. The absorption capacity of RCPs is higher than QS, and the stored moisture is transferred to the matrix, compensating for that consumed because of reactions and evaporation. The geopolymer production is facilitated with internal curing. One of the major components of RCPs is calcite (Fig. 1(b)). Because of the strong acid-base interactions and fine crystal sizes, microcrystalline calcite in RCPs provides nucleation points for the geopolymerisation reactions, as suggested in previous studies [49,50]. The produced C(A)SH can grow on the surface of the crystal nucleus, promoting the reactions [51]. However, the replacement with RCPs potentially inhibits reactions due to the dilution effect (at given mass, the volume of RCPs is larger than QS) [4] and potentially causes a significant increase in unreacted portlandite and calcite in the matrix. The introduction of RCPs decreases the amount of available water in the early stage, inhibiting chemical reactions and decreasing workability [32]. The decreased workability may further prevent fibre dispersion, decreasing strength. In addition, the additional moisture migration channels from the continuous internal pores in RCPs accelerate the water evaporation during curing [52], reducing the available water for reactions. By incorporating MWCNTs, the filler effect partially offsets the additional porosity from RCPs [20], so that higher proportions of RCPs can be incorporated with enhanced geopolymerisation. Compared to a previous study [30], the calcium source in this study is much higher because of a high GGBFS proportion, and portlandite does not significantly participate in the geopolymerisation.

3.2. *Shrinkage behaviour*

3.2.1. *Autogenous shrinkage*

Fig. 5 illustrates the development of autogenous shrinkage of MWCNT-EGC of varying RCPs' proportions with time. The autogenous shrinkage develops rapidly at early stages. The 1-day autogenous

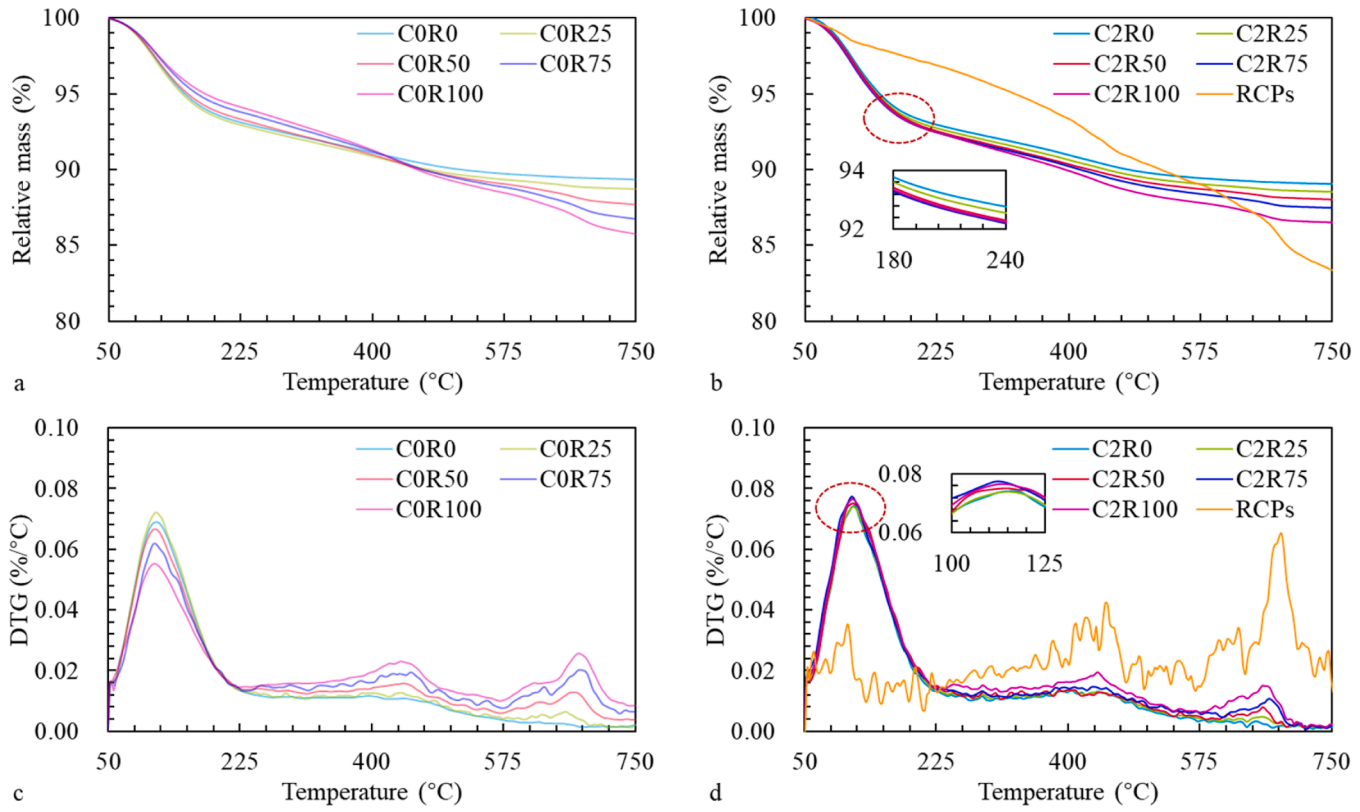

Fig. 4. Effects of RCPs on thermal properties: (a). TGA of EGC, (b). TGA of MWCNT-EGC and RCPs, (c). DTG of EGC, (d). DTG of MWCNT-EGC and RCPs.

Table 5
Effects of RCPs on mass changes in different stages.

Group	Relative mass (%)		
	220 °C	580 °C	700 °C
C0R0	93.18	89.72	89.44
C0R25	93.00	89.30	88.77
C0R50	93.37	89.01	87.89
C0R75	93.85	88.78	87.08
C0R100	94.21	88.44	86.28
C2R0	93.02	89.44	89.14
C2R25	92.80	89.05	88.63
C2R50	92.58	88.67	88.09
C2R75	92.48	88.33	87.53
C2R100	92.52	87.77	86.60
RCPs	96.89	88.89	84.54
Group	Mass loss (%)		
	50–220 °C	250–580 °C	580–700 °C
C0R0	6.82	3.45	0.29
C0R25	7.00	3.70	0.53
C0R50	6.63	4.36	1.12
C0R75	6.15	5.07	1.71
C0R100	5.79	5.78	2.15
C2R0	6.98	3.58	0.30
C2R25	7.20	3.76	0.42
C2R50	7.42	3.91	0.58
C2R75	7.52	4.15	0.80
C2R100	7.48	4.75	1.17
RCPs	3.11	8.00	4.36

shrinkage of EGC and MWCNT-EGC reaches 3954 (C0R100) to 4882 με (C0R0) and 3791 (C2R100) to 4155 με (C2R0), accounting for over 85.9–86.6 % and 83.0–83.6 % of the 28-day autogenous shrinkage. Compared to C2R0 (4977 με), 28-day autogenous shrinkage decreases by 2.5 % (4851 με), 5.3 % (4714 με), 7.3 % (4616 με), and 8.3 % (4566 με) with 25 %, 50 %, 75 %, and 100 % RCPs, respectively. For EGC groups, only 25 % RCPs (5593 με) demonstrate shrinkage mitigation compared to the control group (5683 με). The incorporation of 0.2 % MWCNTs demonstrates mitigation of 90-day autogenous shrinkage of 11.9 % (5004 με). The further replacement of QS with 25 %, 50 %, 75 %, and 100 % RCPs decreases the autogenous shrinkage by 0.9 % (4958 με), 1.7 % (4919 με), 2.9 % (4859 με), and 3.4 % (4833 με), respectively. These values are 12.8 %, 13.4 %, 14.5 %, and 15.0 % lower than the control group.

The autogenous shrinkage results from the self-desiccation because of the geopolymerisation reactions and capillary pressure associated with moisture consumption [53]. The volumes of the geopolymerisation products, i.e., C(A)SH gels, are smaller than the precursors, contributing to volume reduction of EGC [54]. The presence of MWCNTs provides micro-crack bridging capacity and nano-filler effect, which inhibits self-desiccation and pore connectivity, thus reducing autogenous shrinkage [20]. The reduction in the autogenous shrinkage results from the internal curing effect of RCPs [55]. The introduced RCPs release moisture in a prolonged period, effectively compensating for the moisture induced by the geopolymerisation processes [56]. The discharge of moisture from RCPs rather than capillary pores further inhibits the shrinkage development [57]. The inclusion of RCPs potentially decreases the quantity of GGBFS in the reactions because of the dilution effect, slowing down the geopolymerisation in the early period. Additionally, the voids in RCPs can partially relieve the capillary pressure induced by moisture loss, thereby inhibiting the shrinkage development.

On the other hand, the introduction of RCPs promotes the geopolymerisation reactions and C(A)SH productions, as determined in the XRD and TGA-DTG. The promoted formation of C(A)SH contributes to the autogenous shrinkage, offsetting the advantages of internal curing. The high quantity of voids in RCPs results in continuous pores in the matrix, contributing to the shrinkage [58]. However, further C(A)SH production and moisture loss may not significantly increase the autogenous after the formation of the EGC skeleton [32]. Therefore, the addition of RCPs slightly inhibits the development of autogenous shrinkage of EGC and MWCNT-EGC after 90 days.

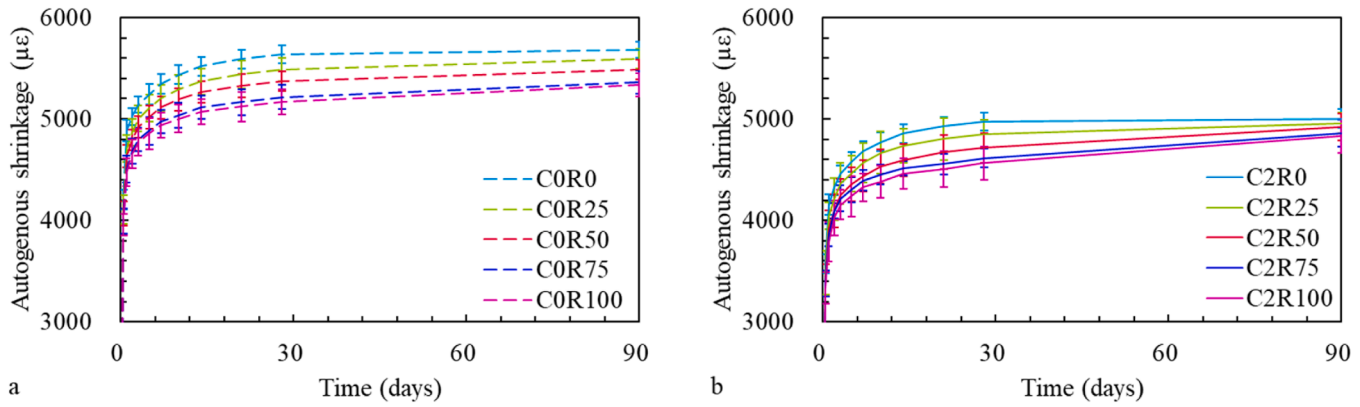

Fig. 5. Effects of RCPs on the autogenous shrinkage of: (a). EGC, (b). MWCNT-EGC.

3.2.2. Drying shrinkage

The mass reduction of EGC and MWCNT-EGC with varying RCPs' contents during curing is demonstrated in Fig. 6(a) and (b), respectively. The introduction of RCPs creates additional moisture transportation channels because of their relatively porous nature, accelerating the water evaporation [59]. Therefore, introducing RCPs increases the water evaporation in the early stage. For example, the complete replacement with RCPs increases the moisture loss by 17 % after 0.5 day. On the other hand, adding RCPs potentially reduces the amount of available moisture to migrate over the longer period due to more stabilised water in geopolymerisation. The mass reduction of EGC and MWCNT-EGC after 90 days is 1.80 %, 1.75 %, 1.86 %, 2.03 %, 2.18 % and 1.73 %, 1.62 %, 1.55 %, 1.46 %, 1.51 % with RCPs' proportion of 0 %, 25 %, 50 %, 75 %, and 100 %, respectively. This is consistent with the XRD and TGA results presented in Sections 3.1.1 and 3.1.2. The replacement with 25 % RCPs in EGC and up to 75 % RCPs in MWCNT-EGC increases C(A)SH formation, indicating that more water can be retained in the gel products, i.e., a reduction in the water available for evaporation.

The corresponding drying shrinkage in response to the water reduction is illustrated in Fig. 6(c) and (d). In the early period, the values of drying shrinkage of MWCNT-EGC are similar to the autogenous shrinkage. After 1 day, the drying shrinkage of MWCNT-EGC varies from 3790 (C2R75) to 4368 με (C2R0) and 4541 με (C0R0). For EGC, the 1-day drying shrinkage ranges from 4356 (C0R25) to 5190 με (C0R100). After 90 days, the corresponding shrinkage values of EGC and MWCNT-EGC with 0 %, 25 %, 50 %, 75 %, and 100 % RCPs are 9497, 9231, 9455, 9705, 10047 με and 8281, 8018, 7697, 7414, 7508 με, respectively. For EGC, only C0R25 exhibits inhibited drying shrinkage. For EGC, only C0R25 exhibits inhibited drying shrinkage because of reduced

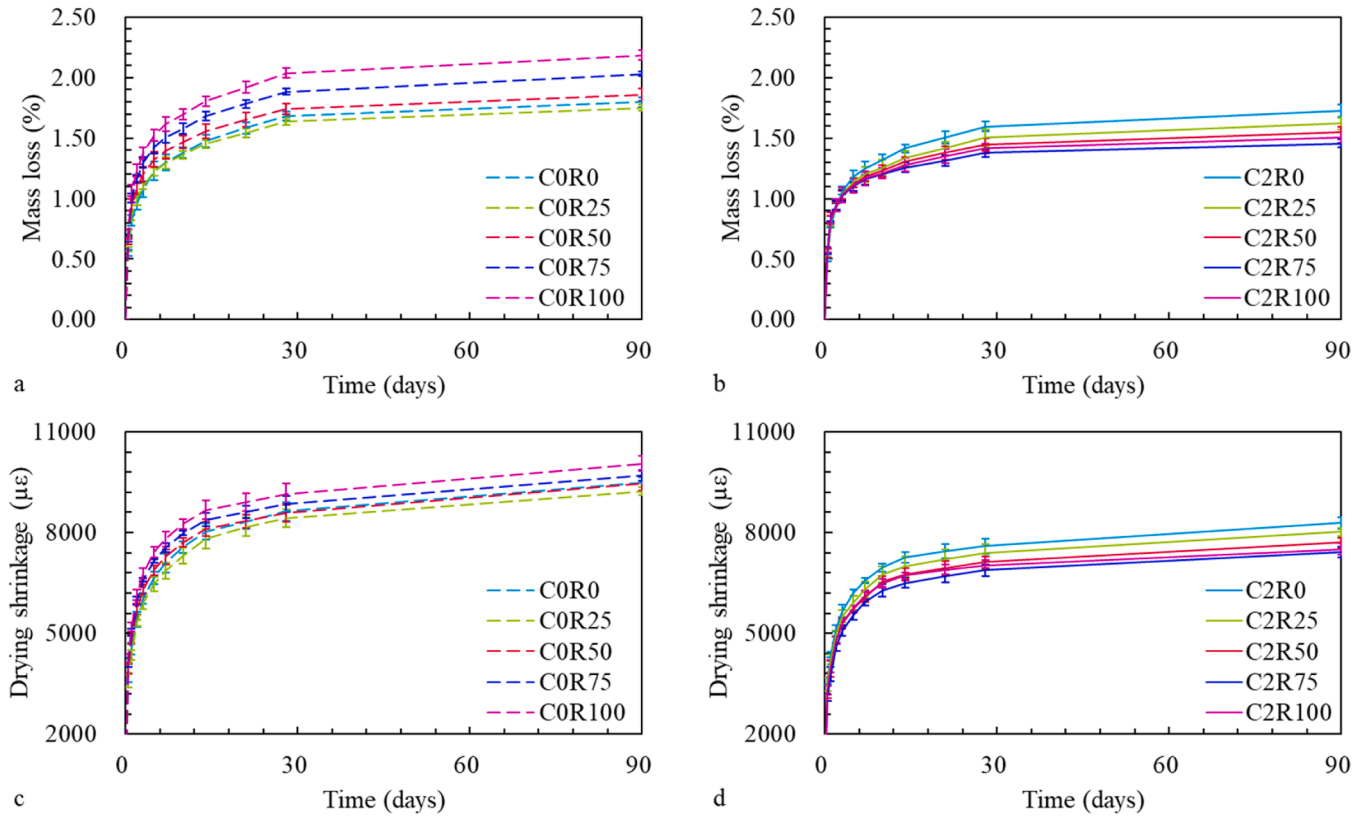

Fig. 6. Effects of RCPs on the drying process: (a). Mass reduction of EGC, (b). Mass reduction of MWCNT-EGC, (c). Drying shrinkage of EGC, (d). Drying shrinkage of MWCNT-EGC.

moisture loss with improved gel production. Compared to C2R0, the 90-day drying shrinkage is mitigated by 3.2 %, 7.0 %, 10.5 %, and 9.3 % with 25 %, 50 %, 75 %, and 100 % RCPs, respectively. The inclusion of 0.2 % MWCNTs and 75 % RCPs inhibits the drying shrinkage of 21.0 % compared to the control group (9497 με). This is attributed to the reduced moisture loss and capillary pressure [60,61]. The development of drying shrinkage of EGC with varying RCPs' proportions is similar to previous studies [58,62,63]. In these studies, the additional water added to RCPs and increased water migration channels increases water migration, promoting drying shrinkage. Although no additional water is used in this study, the incorporation of RCPs increases moisture loss (Fig. 6(a)) because of inhibited reactions, thereby increasing drying shrinkage of EGC with RCPs over 25 %. Additionally, the lower elastic modulus of RCPs compared to QS adversely affects the stiffness of aggregates [64], inhibiting the capacity of the MWCNT-EGC matrix to resist shrinkage.

By contrast, the trend of drying shrinkage with increasing RCPs' proportions in MWCNT-EGC is different from these studies [58,62,63]. There is no additional water to RCPs, and less water could be evaporated from MWCNT-EGC because of the higher water consumption associated with gel production with RCPs. The water loss is the driving factor for the drying shrinkage [63]. The reduced water loss (Fig. 6(b)) offsets the adverse effects of stiffness drop and prevents the development of drying shrinkage [65]. The increased drying shrinkage with RCPs' dosages from 75 % to 100 % can be attributed to the additional moisture transportation channels [66] and inhibited geopolymerisaiton reactions, which increase the moisture evaporation. The trends of varying RCPs' proportions on autogenous and drying shrinkage of MWCNT-EGC were slightly different. The increase of RCPs' content from 75 % to 100 % inhibits the reactions and gel production (Sections 3.1.1 and 3.1.2), which prevents the self-desiccation and capillary tension because of geopolymerisation reactions and decreases autogenous shrinkage [58]. However, owing to additional water loss with 100 % RCPs in MWCNT-EGC, the drying shrinkage can be increased compared to 75 % RCPs.

3.3. Permeable porosity

Fig. 7 illustrates the permeable porosity of MWCNT-EGC. For EGC, the incorporation of 25 % RCPs reduces the permeable porosity from 12.75 % to 12.48 %, whereas the further introduction of RCPs increases the permeable porosity. Because of filler effects [17], the inclusion of 0.2 % MWCNTs decreases the permeable porosity by 6.5 %, reaching 12.01 %. Although RCPs demonstrate higher porosity than QS because of internal pores (Section 2.1), the replacement of QS with RCPs reduces the permeable porosity of MWCNT-EGC. The inclusion of 25 %, 50 %, and 75 % RCPs in MWCNT-EGC further decreases the permeable porosity by 1.5 % (to 11.82 %), 3.9 % (to 11.54 %), and 4.4 % (to 11.48 %), respectively. The significant reduction in permeable voids of C2R75 ($p < 0.05$) indicates a compact matrix, suggesting improved durability in harsh environments, such as chloride attack [67]. The refined pore structure with 0.2 % MWCNTs and 75 % RCPs suggests that the transport of chloride ions could be hindered due to increased tortuosity [68]. By contrast, the inclusion of RCPs in EGC does not significantly reduce the permeable porosity ($p > 0.05$). This can be related to the rapid water exclusion because of additional water transportation channels associated with RCPs, which can be reflected as rapid and higher water evaporation during curing (Section 3.2.2). The enhanced water loss suggests less water is utilised for geopolymerisation reactions, and less gel could be formed [52]. Therefore, the permeable porosity of EGC increases to 16.02 % with 100 % RCPs.

The lower permeable porosity of EGC with 25 % RCPs and MWCNT-EGC with 25–75 % RCPs could result from the enhanced gel production, which fills the capillary pores, increases matrix compactness, and decreases overall porosity [69]. The presence of MWCNTs in the matrix potentially offsets the negative effects of additional voids from RCPs and prolongs the migration of water. Therefore, up to 75 % RCPs can be favourable for gel production in MWCNT-EGC, while only 25 % RCPs facilitate the gel formation. However, as water can be retained in RCPs, the excessive RCPs (100 %) in MWCNT-EGC lead to limited availability of water and alkaline activators in the matrix, preventing geopolymerisation and gel formation [4], which potentially increases the porosity to 12.64 %. The increased permeable porosity with RCPs from 75 % to 100 % is consistent with the inhibited gel production indicated in Sections 3.1.1 and 3.1.2.

3.4. Mechanical performance

3.4.1. Compressive behaviour

The (unconfined) compressive strength of MWCNT-EGC of varying RCPs' percentages is presented in Fig. 8. The introduction of RCPs prolonged the geopolymerisation reactions and strength development, as consistent with the shrinkage development. After 7 and 14 days, the compressive strength of C0R100 and C2R100 is 86 % and 92 %, and 85 % and 90 % of the 28-day strength, respectively. Those ratios are lower than C0R0 and C2R0 with QS (92 % and 96 %). Without MWCNTs, only C0R25 (92.2 MPa) exhibits a 28-day strength increment of 2.8 %. After 28 days, the compressive strength of MWCNT-EGC reaches 100.4 (C2R0) to 120.8 MPa (C2R75). The complete replacement with RCPs decreases the strength to 117.0 MPa. Compared to the control group (89.6 MPa), the incorporation of 0.2 % MWCNTs significantly increases the strength by 12.0 % ($p < 0.05$), and the combined application of 0.2 % MWCNTs and 75 % RCPs enhances the strength by 34.8 %. The combined application of MWCNTs and RCPs demonstrates a significant improvement in the compressive strength than pure MWCNTs or RCPs ($p < 0.05$).

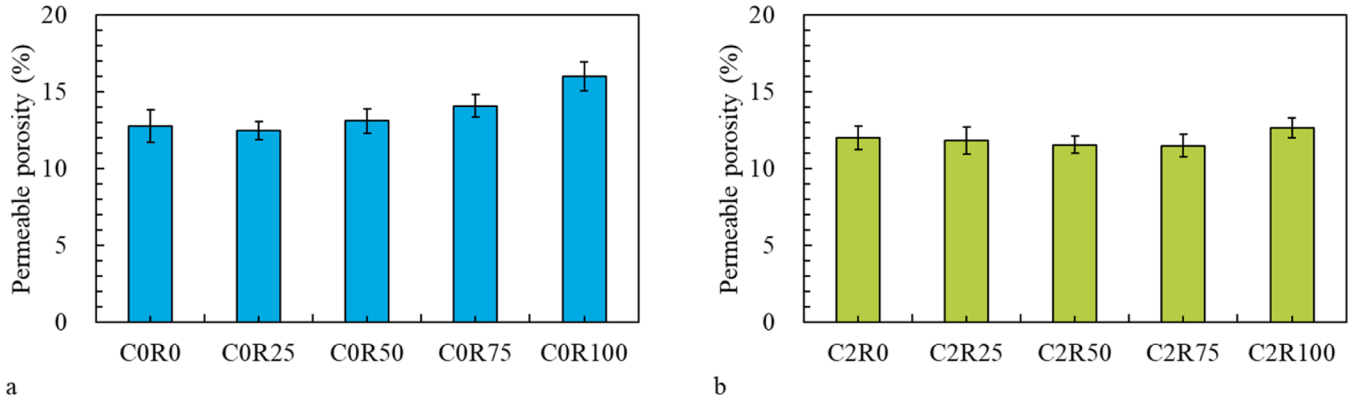

Fig. 7. Effect of RCPs on the permeable porosity of: (a). Pure EGC, (b). MWCNT-EGC.

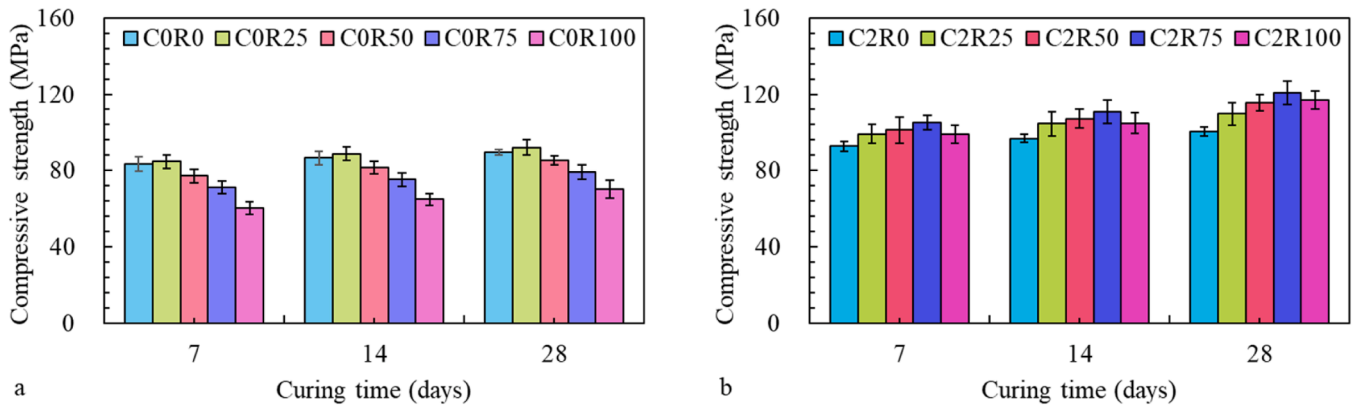

Fig. 8. Effect of RCPs on the compressive strength of: (a). Pure EGC, (b). MWCNT-EGC.

The strength improvement of EGC and MWCNT-EGC with RCPs is attributed to the enhanced secondary geopolymerisation of calcium contents (portlandite) in RCPs in alkaline environments, as suggested in Sections 3.1.1 and 3.1.2. The promoted productions of C(A)SH are beneficial to a compact structure and improved mechanical behaviour [70]. The enhanced C(A)SH formations facilitate the interfacial bonds between aggregates, pastes, and fibres [71]. Besides, the finer sizes of RCPs than QS are favourable for the filler effect, decreasing the macro-pores in the matrix, improving the structure compactness, and enhancing the strength [72]. Although adding RCPs introduces additional micro-pores into the matrix, those voids are effectively bypassed by the surrounding gel network (Section 3.3), minimising the detrimental effects during compression [73]. However, the incorporation of RCPs in EGC does not contribute to a significant strength increment ($p > 0.05$). This difference is likely to be associated with MWCNTs. Although portlandite in RCPs is potentially beneficial for further gel production, the excessive pores in RCPs cause additional water migration channels and rapid moisture evaporation (Section 3.2.2), inhibiting geopolymerisation and gel formation. The SEM results from Liu et al. [74] and Wu et al. [28] indicate that RCPs could reduce the internal micro-cracks and voids in the matrix and refine the micro-structure. The filler effect of MWCNTs offsets the negative effect of these water migration channels from RCPs [12], as consistent with the permeable porosity in Section 3.3. In addition, the incorporated MWCNTs provide bridging, inlaying, and filling effects, disconnecting the voids, inhibiting the development of cracks, and forming a denser micro-structure, which are verified by the SEM results by [61]. Similar SEM results also demonstrate that the incorporation of MWCNTs reduces the unreacted raw materials in the matrix, i.e., enhanced reactions, which contributes to the formation of additional gels [60]. Furthermore, the SEM findings by Wang et al. [75] also demonstrate that the addition of MWCNTs leads to the number and width of microcracks at the interfacial transition zone.

3.4.2. *Tensile behaviour*

Fig. 9 illustrates the normalised stress-strain curves of EGC and MWCNT-EGC containing diverse percentages of RCPs. The peak stress and corresponding strain are scaled by the mean peak stress and average corresponding strain of the 3 replicates. The average first-cracking and ultimate tensile strengths, and strain capacity of EGC and MWCNT-EGC of varying RCPs' proportions are summarised in Table 6. Similar to the compressive strength, the initial crack and ultimate tensile strength of MWCNT-EGC increase when RCPs' proportions are below 75 %. The introduction of 25 %, 50 %, and 75 % RCPs improves the tensile strength by 4.2 % (7.65 MPa), 8.7 % (7.99 MPa), and 11.7 % (8.20 MPa), with corresponding improvement of 22.1 %, 27.4 %, and 30.9 % to the control group (6.27 MPa), respectively. Although the tensile strength decreases with full replacement with RCPs, it is still 9.5 % higher (8.04 MPa) than that with QS (7.34 MPa) and 28.3 % higher than the control group ($p < 0.05$). Similar trends can be observed with the tensile strain, which is improved by 3.6 %, 6.5 %, 8.4 %, and 6.6 % with 25 %, 50 %, 75 %, and 100 % RCPs, which are 12.6 %, 15.6 %, 17.8 %, and 15.9 % higher than the control group (8.46 %), respectively. Furthermore, the replacement with RCPs leads to a larger quantity of fine cracks. The incorporation of 75 % RCPs significantly reduces the mean crack width by 11.2 % (116.0 μm, $p < 0.05$). The improved tensile performance could be attributed to the enhanced gel production and formation of a compact structure due to filler, internal curing, and additional calcium source from RCPs [30,72]. However, for EGC groups, the incorporation of RCPs decreases the tensile strength, strain capacity, number of cracks, and decreases the average crack width regardless of the proportions. The additional voids in RCPs potentially

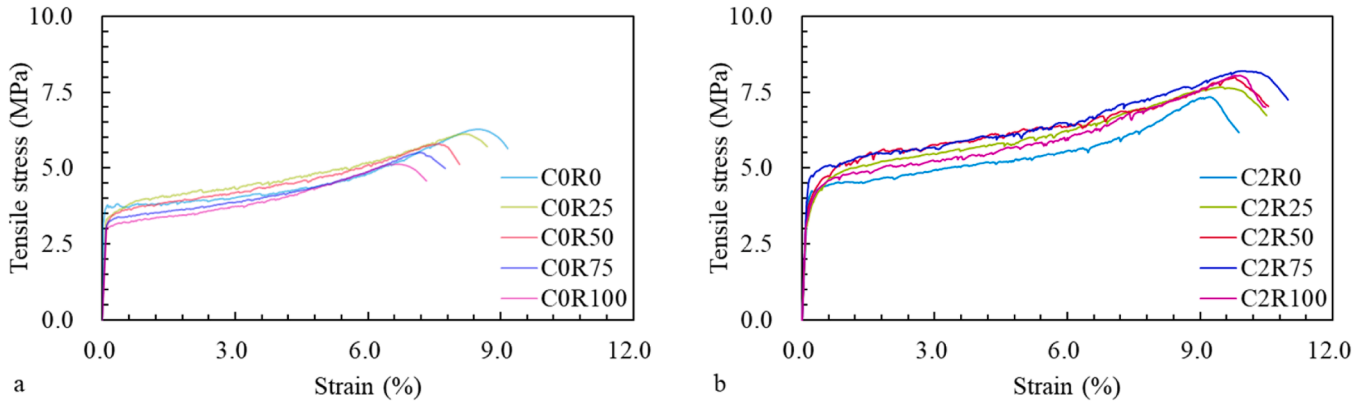

Fig. 9. Effects of RCPs on the tensile performance of: (a). EGC, (b). MWCNT-EGC.

Table 6
Effects of RCPs on the tensile parameters of MWCNT-EGC.

Group	First crack strength (MPa)	Tensile strength (MPa)	Strain capacity (%)	Number of cracks	Crack width (μm)
C0R0	3.66 ± 0.12	6.27 ± 0.26	8.46 ± 0.55	51 ± 5	165.1 ± 5.8
C0R25	3.54 ± 0.16	6.13 ± 0.28	8.13 ± 0.27	48 ± 5	171.3 ± 10.6
C0R50	3.40 ± 0.18	5.80 ± 0.17	7.62 ± 0.20	43 ± 4	179.1 ± 10.1
C0R75	3.24 ± 0.09	5.50 ± 0.21	7.19 ± 0.36	38 ± 4	188.5 ± 12.1
C0R100	3.06 ± 0.11	5.14 ± 0.18	6.68 ± 0.35	34 ± 3	196.9 ± 7.1
C2R0	4.09 ± 0.10	7.34 ± 0.20	9.19 ± 0.22	71 ± 4	130.6 ± 6.4
C2R25	4.31 ± 0.16	7.65 ± 0.22	9.52 ± 0.28	78 ± 6	123.3 ± 8.1
C2R50	4.42 ± 0.32	7.99 ± 0.44	9.78 ± 0.31	83 ± 5	118.9 ± 7.3
C2R75	4.45 ± 0.30	8.20 ± 0.49	9.96 ± 0.56	88 ± 6	116.0 ± 9.5
C2R100	4.39 ± 0.34	8.04 ± 0.33	9.80 ± 0.54	85 ± 4	117.9 ± 7.4

serve as defects and decrease the tensile performance of EGC [32].

The increased compressive and tensile behaviours suggest that replacing QS with RCPs is feasible for enhancing the mechanical properties of MWCNT-EGC. The tensile behaviour of MWCNT-EGC with RCPs is improved due to internal curing, filler, and nucleation effects, as introduced in Section 3.4.1. Besides those mechanisms, the promotion in C(A)SH contributes to improved interfacial bonding between aggregates, pastes, and fibres [32], promoting the tensile performance of MWCNT-EGC. However, the sole application of RCPs in EGC contributes to negative effects on the tensile performance.

3.5. Thermal stability

3.5.1. Mass loss

The variations in the mass change of MWCNT-EGC with varying RCPs' proportions and exposure temperatures are illustrated in Fig. 10. The mass loss increases with the replacement by RCPs. The increased changes in mass are attributed to the promoted water retention and production of C(A)SH associated with RCPs. The production of C(A)SH leads to a compact structure, inhibiting water migration and promoting water retention [33]. Therefore, C0R25 and C2R75 exhibit the highest mass change at 60, 100, and 140 °C, respectively. The promoted C(A)SH production of EGC and MWCNT-EGC with RCPs results in the enhanced dehydroxylation and decomposition of these gels at 400 and 600 °C [31], together with the decomposition of portlandite [33]. Therefore, after 600 °C, the mass loss increases with RCPs' proportions. The mass changes increase with RCP's contents. The mass reduction of EGC ranges from 1.06 % to 1.70 %, 4.23–5.00 %, 7.53–8.15 %, 11.64–12.56 %, and 14.56–17.79 % at 60, 100, 140, 400, and 600 °C, respectively. The corresponding values of MWCNT-EGC vary from 1.79 % to 2.52 %, 5.26–5.64 %, 8.55–9.35 %, 13.12–14.49 %, and 15.38–17.13 % at 60, 100, 140, 400, and 600 °C, respectively.

3.5.2. Residual compressive strength

Fig. 11 (a) and (b) demonstrates the residual compressive strength of EGC and MWCNT-EGC with varying RCPs' dosages and exposed temperatures. The ratios to the strength before exposure are illustrated in Fig. 11 (c) and (d) accordingly. After exposure to 60 and 100 °C, the compressive strength is improved by 3.7–9.7 % and 7.1–20.0 % and 6.7–9.5 % and 15.8–22.0 % for EGC and MWCNT-EGC, respectively. The strength improvements are attributed to enhanced C(A)SH production under elevated temperatures, as determined by XRD tests in previous studies [23,31]. The replacement of QS with RCPs triggers this potential due to additional calcium sources (portlandite). The increment is most significant with 25 % RCPs for EGC and 75 % RCPs for MWCNT-EGC. The enhanced C(A)SH formation with 25 % RCPS in EGC and 75 % RCPs in MWCNT-EGC decreases the water migration and leads to more available free water in the matrix because of the compact structure, as presented in Section 3.5.1. The remaining moisture in the matrix is favourable for the geopolymerisation reactions under the elevated temperatures. The exclusion of moisture associated with chemical reactions and evaporation was beneficial to fibre-matrix bonding, facilitating bridging effects of fibres [76]. Although the geopolymerisation process is promoted, the melting of PE fibres at 140 °C results in strength degradation. The residual strength after 140 °C could increase (C2R75 and C2R100) or decrease slightly (all EGC groups, C2R0, C2R25, and C2R50). The residual strength of C2R75 reaches 150.1 MPa, with an increment of 24.2 % compared to that after curing. The strength is improved by 32.4 % compared to C2R0 (113.4 MPa) and 52.0 % compared to C0R0 (98.8 MPa), respectively.

Under 400 °C, the strength reduction results from the partial decomposition of PE fibres [33] and dehydroxylation of C(A)SH [77]. The shrinkage of the geopolymer matrix and expansion of QS lead to the development of micro-cracks [78]. Compared to 140 °C, the compressive strength of EGC and MWCNT-EGC exhibits a reduction of 12.9–21.9 % and 7.3–10.5 %, respectively. The strength of MWCNT-EGC (105.1–136.9 MPa) is still 4.7–13.4 % higher than that before exposure (100.4–120.8 MPa), whereas all EGC mixes (52.2–91.4 MPa) demonstrate reduced strength compared to that under the ambient temperature (70.3–92.2 MPa). After 600 °C, the complete degradation of PE fibres and C(A)SH leads to significant strength reduction [31]. Although MWCNTs are thermally stable without significant structural change at 600 °C and provide nano-filler and bridging

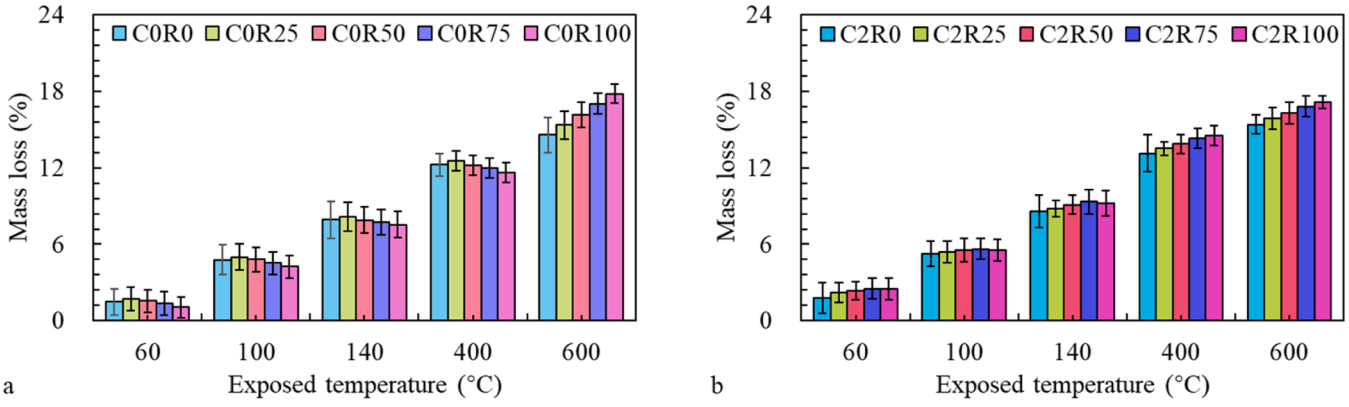

Fig. 10. Effects of RCPs on the mass changes after heat exposures: (a). EGC, (b). MWCNT-EGC.

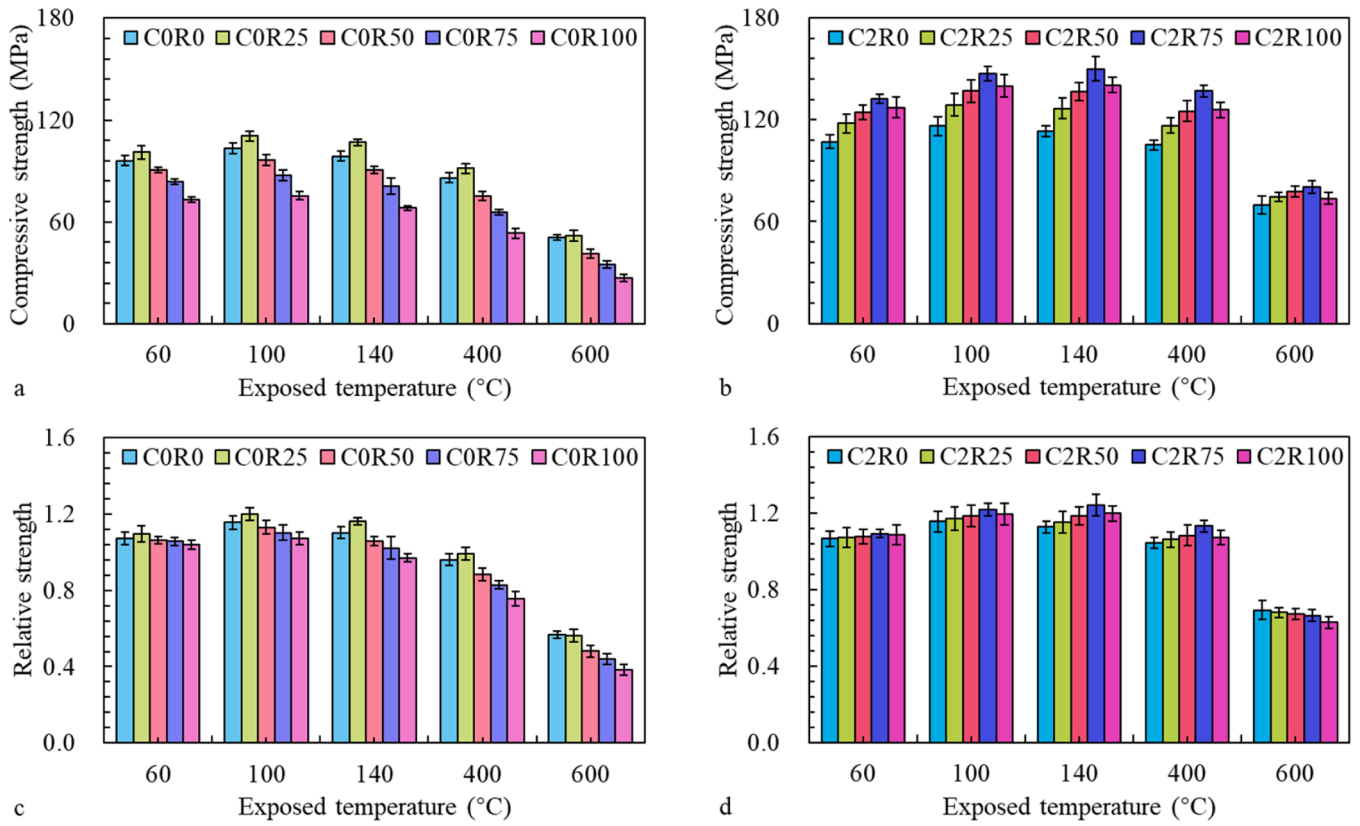

Fig. 11. Effects of RCPs on the residual compressive behaviour after thermal exposures: (a). Residual compressive strength of EGC, (b). Residual compressive strength of MWCNT-EGC, (a). Relative compressive strength of EGC, (b). Relative compressive strength of MWCNT-EGC.

effects [12], the strength is decreased by 33.7–41.4 % from 400 °C because of continuous degradation of C(A)SH gels [33]. The residual strength (27.0–80.4 MPa) ranges from 38.3 % (C0R100) to 69.4 % (C2R0) of that before exposure. It is highlighted that MWCNT-EGC with 25 %, 50 %, 75 %, and 100 % RCPs exhibits significant strength improvement of 7.2 %, 11.3 %, 15.3 %, and 5.7 % compared to C2R0 and 47.1 %, 52.8 %, 58.2 %, and 45.1 % ($p < 0.05$) compared to C0R0, respectively. The higher residual strength can be attributed to the filler effect and compact structure of RCPs. The fine particle sizes and promoted C(A)SH productions are favourable for the matrix compactness, inhibiting the potential for initiation and development of micro-cracks, enhancing strain-hardening behaviour [79]. The MWCNT-EGC with 75 % RCPs exhibit 58.2 % improvement in the residual compressive strength compared to the control group (50.8 MPa).

3.5.3. *Residual tensile performance*

The normalised stress-strain behaviour of MWCNT-EGC with varying RCPs' contents is presented in Fig. 12 (a), (b), and (c), after the thermal exposure of 60, 100, and 140 °C, respectively. The residual tensile strength and strain capacity, and tensile strength retention are presented in Fig. 12 (d), (e), and (f), respectively. The results reveal that MWCNTs significantly increase thermal durability of EGC ($p < 0.05$), and tensile behaviour of MWCNT-EGC depends on RCPs' proportions. The tensile performance is improved due to enhanced gel productions but deteriorates because of softening or melting of PE fibres [80]. The promoted gel production under the elevated temperatures is beneficial for a compact matrix, which increases the bonding between fibres and matrix [70]. Same as that explained in Section 3.5.2, the existence of RCPs provides an additional calcium source (portlandite) for further geopolymerisation reactions under a steaming condition created at elevated temperatures [33], and the removal of moisture further enhances the bonding between fibres and matrix [81]. It should be highlighted that the improvements are more significant with relatively high RCPs' contents, as higher portlandite can be included in reactions, which potentially forms more gel products and improves the fibre-matrix bonding [82]. In addition to those mechanisms, initiation of micro-cracks at elevated temperatures is beneficial to multi-cracking behaviour, enhancing the strain capacity of MWCNT-EGC [70].

Although the above mechanisms are favourable for the tensile properties of MWCNT-EGC, the softening and melting of PE fibres after 60 and 140 °C deteriorate tensile performance, as the softened or molten fibres may be subjected to shape changes under the elevated temperatures, when the matrix exhibits volumetric shrinkage [33]. The fibres could partially lose the function (i.e., bridging and crack control capacity) because of shape change [70]. Therefore, increasing temperatures can exert both beneficial and adverse effects on the tensile behaviour of MWCNT-EGC, whereas the overall outcome depends on the relative dominance of these competing mechanisms. The tensile strength is promoted at 60 and 100 °C, despite RCPs' dosages or incorporation of MWCNTs. The elevated temperatures lead to enhanced geopolymerisation reactions [83], which strengthen the EGC matrix, refine microstructures, and improve the interfacial bonding between fibres and matrix [70]. The residual tensile strengths are 6.59, 7.88, 8.39, 8.92, 9.33, and 9.01 MPa for C0R0, C2R0, C2R25, C2R50, C2R75, and C2R100 at 100 °C, respectively. The corresponding increments are 13.0, 15.4 %, 16.6 %, 17.9 %, and 16.0 %, respectively (Fig. 12 (f)). Those values drop as temperatures increase to 140 °C for C0R0 (6.16 MPa), C2R0 (7.59 MPa), and C2R25 (8.22 MPa). The residual strength of C2R50 (8.91 MPa), C2R75 (9.49 MPa), and C2R100 (9.04 MPa) maintains similar values or exhibits a slight increment compared to that at 100 °C. Although tensile strength could increase upon exposure to elevated temperatures, tensile strain is more sensitive to softening and melting of PE fibres, especially those with lower RCPs' proportions, as consistent with previous results [23,30,70]. The strain capacity of C0R0,

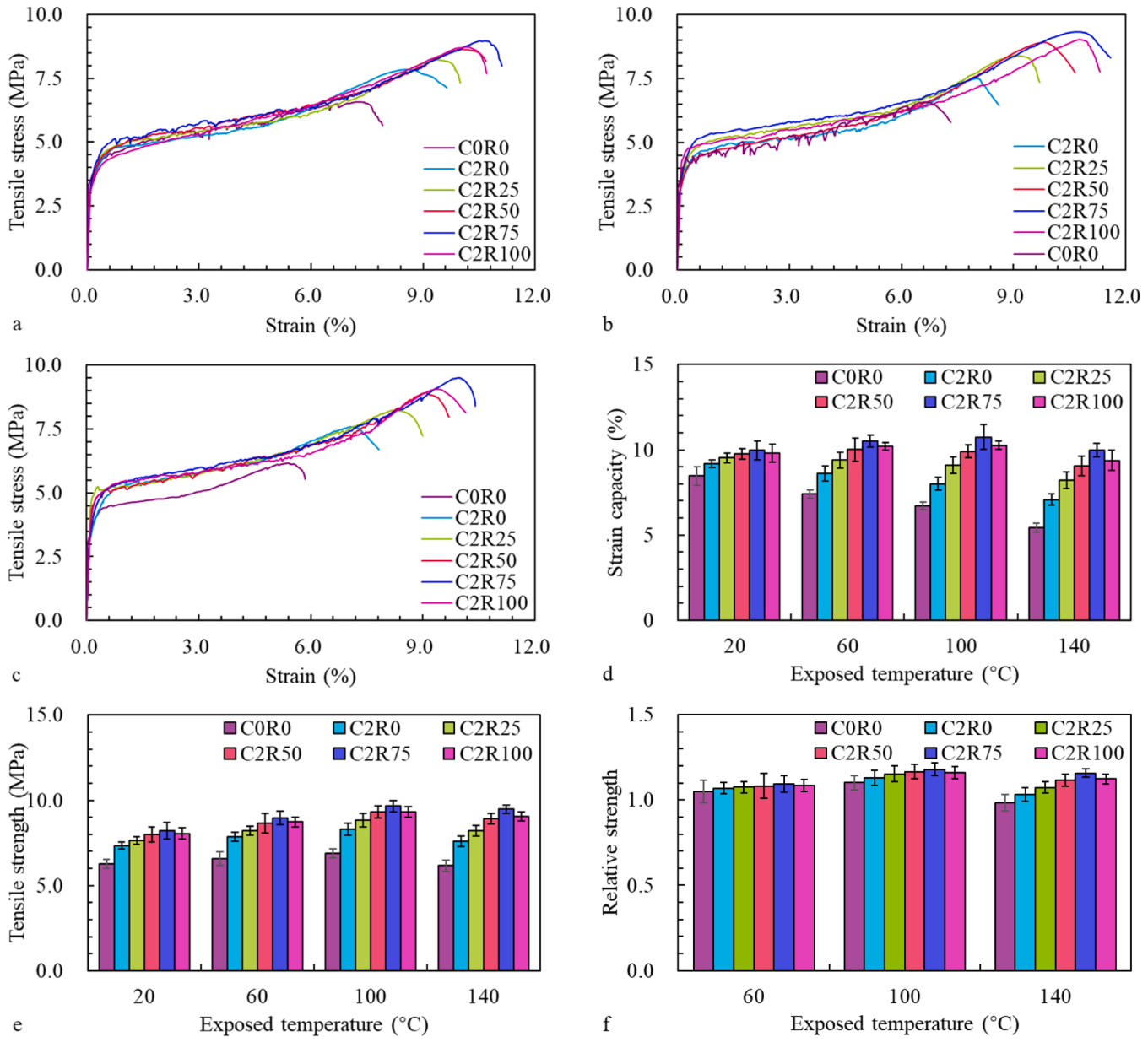

Fig. 12. Effects of RCPs on the tensile performance of MWCNT-EGC after thermal exposures: (a). Tensile performance at 60 °C, (b). Tensile performance at 100 °C, (c). Tensile performance at 140 °C, (d). Strain capacity at varying temperatures, (e). Tensile strength at varying temperatures, (f). Relative tensile strength at varying temperatures.

C2R0 and C2R25 decreases with rising temperatures, whereas that of C2R75 and C2R100 increases at 60 and 100 °C. At 140 °C, the strain capacity of all groups declines substantially, with the most significant strain reductions of 35.9 % for C0R0 and 22.9 % for C2R0, respectively. It can be highlighted that C2R75 exhibits a residual strain capacity of 9.98 %, comparable to that under ambient temperature (9.96 %) after thermal exposure to 140 °C. The tensile strength of C2R75 (9.49 MPa) demonstrates significant improvement of 15.7 % before exposure ($p < 0,05$). The residual tensile strength and strain capacity of C2R75 after being exposed to 140 °C are 54.0 % and 84.1 % higher than the control group, whose values are 6.31 MPa and 5.42 %, respectively.

The variations in the tensile parameters are summarised in Table 7, including crack numbers and widths. With rising temperatures, the cracking numbers increase initially and then decrease due to deterioration of PE fibres, which limits fibres' bridging and crack-control capacity [70], with trends similar to strain capacity. The corresponding cracking widths can be finer or coarser, depending on exposed temperatures and RCPs' proportions. The above results indicate that incorporating RCPs is favourable for residual compressive and tensile performance after elevated temperatures due to enhanced gel production and formation of compact structure, and C2R75 exhibits the highest residual strength and strain among all groups at each temperature.

3.6. Economic and environmental assessment

The unit costs of conventional EGC and MWCNT-EGC of varying RCPs' contents are demonstrated in Fig. 13 (a), and Fig. 13 (b) illustrates the carbon emissions included in the virgin materials for MWCNT-EGC with varying RCPs' proportions, together with those groups without MWCNTs, i.e., conventional EGC. The marker other refers to the sum of QS, SP, and RCPs. Those fractions are combined, otherwise difficult to be distinguished due to low costs and embodied carbon. The detailed quantity from each component is summarised in Table 8 and Table 9 accordingly. For unit volume, the consumption of PE fibres is constant,

Table 7
Effects of RCPs on the tensile parameters of MWCNT-EGC after thermal exposures.

Group	Temperature (°C)	First crack strength (MPa)	Tensile strength (MPa)	Strain capacity (%)	Number of cracks	Crack width (μm)
C0R0	60	4.36 ± 0.24	7.57 ± 0.41	7.40 ± 0.25	45 ± 3	165.5 ± 9.8
C2R0		4.81 ± 0.12	7.85 ± 0.25	8.61 ± 0.43	62 ± 4	142.6 ± 9.7
C2R25		5.11 ± 0.32	8.22 ± 0.26	9.40 ± 0.47	76 ± 6	126.6 ± 10.4
C2R50		5.16 ± 0.41	8.64 ± 0.58	10.00 ± 0.69	85 ± 7	119.8 ± 12.1
C2R75		5.24 ± 0.32	8.97 ± 0.39	10.50 ± 0.36	94 ± 5	113.3 ± 6.3
C2R100		5.19 ± 0.46	8.73 ± 0.30	10.21 ± 0.23	88 ± 6	117.5 ± 7.7
C0R0	100	4.27 ± 0.26	6.59 ± 0.27	6.72 ± 0.23	37 ± 3	182.9 ± 13.6
C2R0		4.66 ± 0.23	7.88 ± 0.36	8.01 ± 0.36	52 ± 4	156.7 ± 11.7
C2R25		4.97 ± 0.30	8.39 ± 0.38	9.09 ± 0.50	69 ± 5	135.8 ± 11.8
C2R50		5.06 ± 0.20	8.92 ± 0.35	9.91 ± 0.39	81 ± 5	124.3 ± 7.9
C2R75		5.17 ± 0.34	9.33 ± 0.34	10.75 ± 0.74	98 ± 4	113.2 ± 6.7
C2R100		5.11 ± 0.31	9.01 ± 0.30	10.26 ± 0.24	86 ± 5	120.6 ± 7.6
C0R0	140	4.32 ± 0.39	6.16 ± 0.35	5.42 ± 0.26	28 ± 2	195.5 ± 15.9
C2R0		4.62 ± 0.25	7.59 ± 0.32	7.08 ± 0.34	40 ± 3	179.6 ± 15.6
C2R25		4.98 ± 0.37	8.22 ± 0.30	8.22 ± 0.49	55 ± 5	152.8 ± 15.0
C2R50		5.03 ± 0.33	8.91 ± 0.32	9.05 ± 0.59	68 ± 6	137.9 ± 14.3
C2R75		5.19 ± 0.27	9.49 ± 0.25	9.98 ± 0.41	83 ± 5	122.9 ± 8.6
C2R100		5.12 ± 0.42	9.04 ± 0.27	9.37 ± 0.59	72 ± 5	133.9 ± 11.9

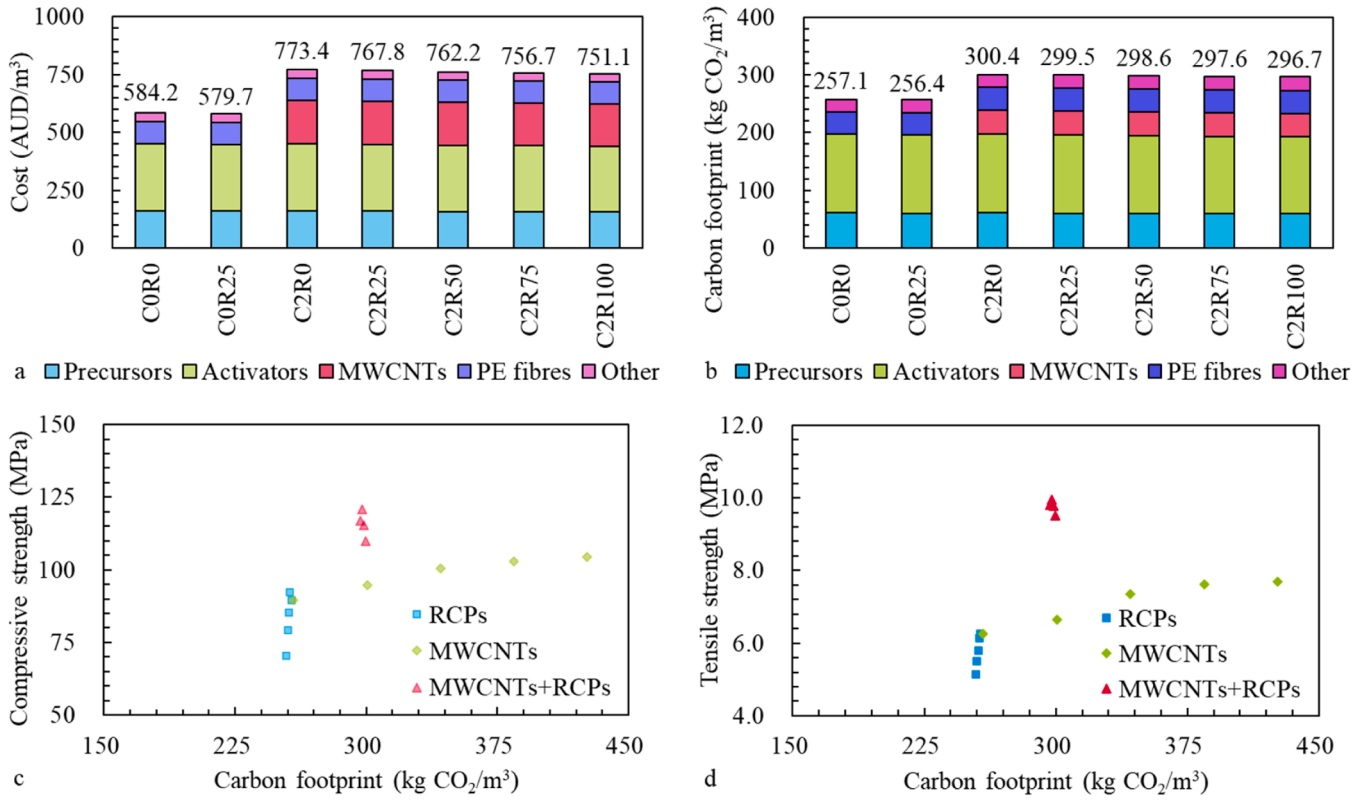

Fig. 13. Effects of RCPs on the economic and environmental impacts of MWCNT-EGC: (a). Unit costs, (b). Carbon emissions, (c). Comparison of compressive strength with the literature, (d). Comparison of tensile strength with the literature.

Table 8
Effects of RCPs on the unit costs of MWCNT-EGC.

Materials	C0R0	C2R25	C0R50	C0R75	C0R100	C2R0	C2R25	C2R50	C2R75	C2R100
GGBFS	134.4	133.6	132.8	132.0	131.2	134.4	133.6	132.8	132.0	131.2
FA	25.2	25.1	24.9	24.8	24.6	25.2	25.1	24.9	24.8	24.6
NS	18.9	14.1	9.3	4.6	0.0	18.9	14.1	9.3	4.6	0.0
RCPs	0.0	3.1	6.2	9.3	12.3	0.0	3.1	6.2	9.3	12.3
SH	37.8	37.6	37.4	37.1	36.9	37.8	37.6	37.4	37.1	36.9
SS	252.0	250.5	249.0	247.5	246.0	252.0	250.5	249.0	247.5	246.0
SP	18.9	18.8	18.7	18.6	18.5	18.9	18.8	18.7	18.6	18.5
PE fibres	97.0	97.0	97.0	97.0	97.0	97.0	97.0	97.0	97.0	97.0
MWCNTs	0.0	0.0	0.0	0.0	0.0	189.0	187.9	186.8	185.6	184.5
Sum	584.2	579.7	575.3	570.9	566.5	773.2	767.6	762.0	756.5	751.0

whereas the introduction of RCPs decreases the consumptions of precursors, alkaline activators, and MWCNTs because of reduced overall density, leading to reduced unit cost and carbon emissions.

The overall costs of EGC of 0.2 % MWCNTs decrease from 773.4 to 751.1 AUD/m^3 (by 2.9 %) with RCPs' contents ranging from 0 % to 100 %. These values are 28.6–32.4 % higher than the control group (584.2 AUD/m^3). The costs to achieve unit compressive and tensile strength output of C0R0 and C0R25 are 6.52 and 93.2 AUD/MPa, and 6.29 and 94.6 AUD/MPa, respectively. Without RCPs, the incorporation of 0.2 % MWCNTs increases the costs to reach unit strength, with corresponding values of 7.70 and 105.3 AUD/MPa, respectively. The lowest prices to attain unit compressive and tensile strength are observed with 0.2 % MWCNTs and 75 % RCPs, with corresponding values of 6.26 and 92.3 AUD/MPa, respectively. The reduced price to reach unit strength indicates that incorporating RCPs partially solves the issues raised by the high cost of MWCNTs.

Similar to unit costs, the carbon emissions of EGC of 0.2 % MWCNTs are reduced from 300.4 to 296.7 kg CO_2/m^3 (by 1.2 %) with RCPs' proportion rising from 0 % to 100 %. However, these values are 15.4–16.9 % higher than the control group (257.1 kg CO_2/m^3) or 15.7–17.2 % higher than EGC with 25 % RCPs (256.4 kg CO_2/m^3). The carbon footprints required to achieve unit compressive (2.99 kg CO_2/MPa) and tensile strength (41.0 kg CO_2/MPa) of C2R0 are close to those of C0R0 (2.87 and 41.0 kg CO_2/MPa) and C0R25 (2.78 and 41.8 kg CO_2/MPa). The inclusion of 75 % RCPs further decreases these values to 2.46 and 36.9 kg CO_2/MPa, respectively. The compressive and tensile strengths of EGC are correlated with carbon footprint, with reference to varying MWCNTs [23], and RCPs, MWCNTs+RCPs (this study). The inclusion of RCPs in MWCNT-EGC demonstrates more significant improvements in compressive and tensile strengths than the addition of RCPs or MWCNTs alone. In addition to the reduced cost and emission to achieve unit strength, the significantly improved performance at elevated temperatures of RCPs-incorporated MWCNT-EGC suggests that introducing RCPs is a cost-effective and environmentally friendly approach to facilitating the mechanical properties and thermal stability of MWCNT-EGC.

4. Limitations and future study

Although this study has verified the economic and environmental values of the incorporation of MWCNTs and RCPs to produce cost-effective and environmentally sustainable EGC, one major limitation of this study is the durability of EGC, such as resistance to multiple freeze-thaw cycles and chloride attack. Although resistance to chloride attack is not directly determined, the reduced permeable porosity of EGC with 0.2 % MWCNTs and 75 % RCPs potentially suggests that the movement of chloride ions can be hindered because of increased tortuosity and inhibited pore connectivity [67]. Zhang et al. [84] summarise the performance of geopolymer with different mix proportions under multiple freeze-thaw cycles and indicate that the higher proportion of calcium is favourable to the resistance to freeze-thaw cycles, and replacement of aggregate with RCAs may slightly reduce the resistance of geopolymer to freeze-thaw cycles [85–87]. The incorporation of MWCNTs is beneficial to the freeze-thaw resistance of geopolymer because of interlocking, filler, and nucleation effects associated with MWCNTs [21,88]. Therefore, the additional calcium source in RCPs and beneficial effects of MWCNTs could potentially facilitate the resistance of EGC to freeze-thaw cycles. In addition, the particle sizes of RCPs can significantly affect the performance of geopolymer, and finer particle sizes of recycled aggregates increase the mechanical properties [37]. The performance of EGC with varying dosages and particle sizes of MWCNTs and RCPs could be further investigated.

5. Summary and conclusion

This study explores the feasibility of recycled concrete powders (RCPs) on the feasibility to improving the shrinkage, mechanical, and thermal behaviours of conventional engineered geopolymer composites (EGC) and 0.2 % multi-walled carbon nanotubes (MWCNT) reinforced engineered geopolymer composites (MWCNT-EGC). Based on the comprehensive laboratory investigation, the following conclusions can be derived.

The inclusion of RCPs mitigates the development of autogenous and drying shrinkage due to filler and internal curing effects, in addition to the reinforcing and bridging effects of MWCNTs. The combined application of 0.2 % MWCNTs and 75 % RCPs decreases the 90-day autogenous and drying shrinkage by 14.5 % and 21.9 % compared to the control group.

The incorporation of 0.2 % MWCNTs and 75 % RCPs contributes to the optimum compressive strength (120.8 MPa), tensile strength (8.20 MPa), and strain capacity (9.96 %), with corresponding improvements of 20.3 %, 11.7 %, and 8.4 % from that without RCPs and 34.8 %, 30.9 %, and 17.8 % from the control group, respectively. The promoted gel production because of additional portlandite in RCPs is revealed by XRD and TGA results.

The thermal resistance of EGC is enhanced by the combined incorporation of 0.2 % MWCNTs and 75 % RCPs. After 600 °C, the residual compressive strength of EGC with 75 % RCPs (80.4 MPa) is 15.3 % higher than that without RCPs (69.7 MPa) and 58.2 % higher than the control group (50.8 MPa), respectively. After 140 °C, the maximum tensile strength (9.49 MPa) and strain capacity (9.98 %) are achieved with 0.2 % MWCNTs and 75 % RCPs, which are 25.0 % and 40.8 % higher than those without RCPs and 54.0 % and 84.1 % higher than the control group, respectively.

The cost-benefit analysis and carbon footprint assessment suggest that introducing RCPs in MWCNT-EGC slightly reduces unit costs and carbon emissions from virgin materials. Although the addition of MWCNTs significantly increases unit price and carbon footprint of EGC, the mix design with 0.2 % MWCNTs and 75 % RCPs exhibits improved cost-effectiveness and sustainability compared to pure EGC with varying RCPs' proportion but without MWCNTs.

With the presented improvements in shrinkage, mechanical, thermal properties, and sustainability compared to the control EGC and MWCNT-EGC, RCPs can be an economically affordable and environmentally friendly material for MWCNT-EGC production. Replacing 75 % QS with RCPs contributes to optimum mechanical performance and

Table 9
Effects of RCPs on the carbon emissions of MWCNT-EGC.

Materials	C0R0	C2R25	C0R50	C0R75	C0R100	C2R0	C2R25	C2R50	C2R75	C2R100
GGBFS	58.8	58.5	58.1	57.8	57.4	58.8	58.5	58.1	57.8	57.4
FA	2.1	2.1	2.1	2.1	2.1	2.1	2.1	2.1	2.1	2.1
NS	15.1	11.3	7.5	3.7	0.0	15.1	11.3	7.5	3.7	0.0
RCPs	0.0	4.4	8.7	13.0	17.2	0.0	4.4	8.7	13.0	17.2
SH	45.1	44.8	44.6	44.3	44.0	45.1	44.8	44.6	44.3	44.0
SS	91.0	90.5	90.0	89.4	88.9	91.0	90.5	90.0	89.4	88.9
SP	6.1	6.1	6.1	6.0	6.0	6.1	6.1	6.1	6.0	6.0
PE fibres	38.8	38.8	38.8	38.8	38.8	38.8	38.8	38.8	38.8	38.8
MWCNTs	0.0	0.0	0.0	0.0	0.0	42.0	41.8	41.5	41.3	41.0
Sum	257.1	256.4	255.7	255.1	254.4	299.1	298.2	297.2	296.3	295.4

thermal stability. However, this study did not investigate the long-term durability of MWCNT-EGC under various hazardous conditions. Further study could be conducted to evaluate the durability of MWCNT-EGC with various proportions and sizes of RCPs and under different types and concentrations of salt solutions.

CRediT authorship contribution statement

Aziz Ahmed: Writing – review & editing, Formal analysis, Conceptualization. **Y.X. Zhang:** Writing – review & editing, Formal analysis, Conceptualization. **Yuekai Xie:** Writing – review & editing, Writing – original draft, Investigation, Formal analysis, Conceptualization.

Declaration of Competing Interest

The authors declare that they have no known competing financial interests or personal relationships that could have appeared to influence the work reported in this paper.

Acknowledgements

This project is financially supported by ARC Industrial Transformation Training Centres for Whole Life Design of Carbon Neutral Infrastructure (IC230100015).

Data availability

Data will be made available on request.

References

[1] Y.-X. Zhang, Y.-H. Gao, R. Lin, W. Hou, G.-W. Yan, J.-R. Lan, L.-Y. Xu, B.-T. Huang, Tuning superior hydrophobic performance of Engineered/Strain-Hardening Cementitious Composites (ECC/SHCC) via polydimethylsiloxane-based bulk modification, Mater. Des. (2025) 114117.
[2] Z. Tang, Y. Zhang, Y. Ding, W. Chen, Y. Jiang, Y. Zhang, N. Ukrainczykc, K. Yu, Insights on the bond behavior between HS-ECC and steel bar: experiment, 3D meso-scale numerical model and probabilistic predictions, Eng. Struct. 343 (2025) 121012.
[3] M.T. Bashir, A.B. Khan, M.M.H. Khan, K. Rasheed, S. Saad, F. Farid, Evaluating the implementation of green building materials in the construction sector of developing nations, J. Hum. Earth Future 5 (3) (2024) 528–542.
[4] Y. Xie, H. Wang, Y. Guo, C. Wang, H. Cui, J. Xue, Mechanical performance and water resistance of biochar admixture lightweight magnesium oxychloride cement, Sci. Total Environ. 912 (2024) 168773.
[5] S. Rawat, Y.X. Zhang, C. Lee, Multi-response optimization of hybrid fibre engineered cementitious composite using Grey-Taguchi method and utility concept, Constr. Build. Mater. 319 (2022) 126040.
[6] L.A. Zghair, M.Z. Yousif, L.K. Salman, R.K.S. Al-Hamd, M.M. Sarhan, Use of recycled ceramic powder as a green alternative in mortar-based cementitious composites, Civ. Eng. J. 10 (10) (2024) 3157–3172.
[7] K. Midhin, L. Wong, Investigating mechanical properties of metakaolin-based geopolymer concrete optimized with wastepaper ash and plastic granules, Civ. Eng. J. (2024).
[8] F. Wang, Y. Ding, T. Nishiwaki, Z. Zhang, J. Yu, K. Yu, Fully recycled engineered geopolymer composite: mechanical properties and sustainability assessment, J. Clean. Prod. 471 (2024) 143382.
[9] Z. Gao, P. Zhang, X. Dai, Y. Zheng, H. Feng, Assessment of bonding behavior of hybrid fiber alkali-activated concrete for tunnel lining concrete restoration, J. Clean. Prod. (2025) 145803.
[10] Y. Sun, J. Cai, L. Xu, X. Ma, J. Pan, Mechanical and environmental performance of engineered geopolymer composites incorporating ternary solid waste, J. Clean. Prod. 441 (2024) 141065.
[11] H. Zhong, M. Zhang, Engineered geopolymer composites: a state-of-the-art review, Cem. Concr. Compos. 135 (2023) 104850.
[12] X. Chen, H. Xiang, S. Li, Z. Cheng, Tensile properties and microstructure of lightweight engineered geopolymer composites containing PVA fibers and multi-walled carbon nanotubes (MWCNTs) after high-temperature exposure, Constr. Build. Mater. 474 (2025) 141154.
[13] R. Krishna, S. Mishra, N. Sethy, S.M. Mustakim, R. Boopathy, S. Rawat, T. S. Qureshi, Impact of high-temperature exposure on the thermal and physio-mechanical performance of graphene-reinforced geopolymer composites, Constr. Build. Mater. 489 (2025) 142285.
[14] S.M. Mustakim, S.K. Das, J. Mishra, A. Aftab, T.S. Alomayri, H.S. Assaedi, C. R. Kaze, Improvement in fresh, mechanical and microstructural properties of fly ash-blast furnace slag based geopolymer concrete by addition of nano and micro silica, Silicon 13 (2021) 2415–2428.
[15] Z. Feng, P. Zhang, J. Guo, Y. Zheng, S. Hu, Single and synergistic effects of nano-SiO2 and hybrid fiber on rheological property and compressive strength of geopolymer concrete, Constr. Build. Mater. 472 (2025) 140945.
[16] O. Khouchani, A. Harmal, T. El-Korchi, M. Tao, H.W. Walker, Effect of cellulose nanocrystals on performance of PVA fiber-reinforced geopolymer composites: reaction kinetics, bending behavior, and toughening mechanisms, Constr. Build. Mater. 435 (2024) 136727.
[17] K. Kishore, M.N. Sheikh, M.N. Hadi, Functionalization of carbon nanotubes for enhanced dispersion and improved properties of geopolymer concrete: a review, J. Build. Eng. (2025) 113096.
[18] R.S. Raj, G.P. Arulraj, N. Anand, B. Kanagaraj, E. Lubloy, M. Naser, Nanomaterials in geopolymer composites: a review, Dev. Built Environ. 13 (2023) 100114.
[19] K. Kishore, M.N. Sheikh, M.N. Hadi, Doped multi-walled carbon nanotubes and nanoclay based-geopolymer concrete: an overview of current knowledge and future research challenges, Cem. Concr. Compos. 154 (2024) 105774.
[20] F. Li, Z. Zhou, Y. Lu, S. Li, Effect of PVA fibers grafted with MWCNTs on the shrinkage behaviors of engineered geopolymer composite (EGC), Constr. Build. Mater. 449 (2024) 138508.
[21] Z. Yang, Z. Liu, F. Li, Y. Lu, S. Li, Effect of multi-walled carbon nanotubes on durability of high-strength slag-based geopolymer, Ceram. Int. 49 (8) (2023) 11936–11949.
[22] H.Y. Teah, T. Sato, K. Namiki, M. Asaka, K. Feng, S. Noda, Life cycle greenhouse gas emissions of long and pure carbon nanotubes synthesized via on-substrate and fluidized-bed chemical vapor deposition, ACS Sustain. Chem. Eng. 8 (4) (2020) 1730–1740.
[23] Y. Xie, Enhanced mechanical and thermal performance of high-strength engineered geopolymer composites reinforced by hybrid polyethylene fibres and carbon nanotubes, Constr. Build. Mater. 472 (2025) 140884.
[24] B. Li, S. Yu, B. Gao, Y. Li, F. Wu, D. Xia, Y. Chi, S. Wang, Effect of recycled aggregate and steel fiber contents on the mechanical properties and sustainability aspects of alkali-activated slag-based concrete, J. Build. Eng. 66 (2023) 105939.
[25] D. Kryeziu, F. Selmani, A. Mujaj, I. Kondi, Recycled concrete aggregates: a promising and sustainable option for the construction industry, J. Hum. Earth Future 4 (2) (2023) 166–180.
[26] F. Wang, J. Zhai, E. Kan, B. Norkulov, Y. Ding, J. Yu, K. Yu, Value-added recycling of waste brick powder and waste sand to develop eco-friendly engineered geopolymer composite, Case Stud. Constr. Mater. 21 (2024) e03590.
[27] Q. Wang, Y.-Y. Wang, Y. Geng, H. Zhang, Experimental study and prediction model for autogenous shrinkage of recycled aggregate concrete with recycled coarse aggregate, Constr. Build. Mater. 268 (2021) 121197.
[28] H. Wu, X. Liu, C. Wang, Y. Zhang, Z. Ma, Micro-properties and mechanical behavior of high-ductility engineered geopolymer composites (EGC) with recycled concrete and paste powder as green precursor, Cem. Concr. Compos. 152 (2024) 105672.
[29] C. Wang, Z. Zhang, X. Liu, Y. Zhang, Z. Ma, Elucidating the role of recycled concrete aggregate in ductile engineered geopolymer composites: Effects of recycled concrete aggregate content and size, J. Build. Eng. 95 (2024) 110150.
[30] Y. Xie, Y. Guo, J. Xue, Development of a sustainable engineered geopolymer composite with mitigated autogenous shrinkage, enhanced mechanical performance, and improved thermal behaviour by recycled concrete powder, Powder Technol. (2025) 121087.
[31] Y. Xie, C. Wang, Y. Guo, H. Cui, J. Xue, Improved mechanical and thermal properties of sustainable ultra-high performance geopolymer concrete with cellulose nanofibres, J. Build. Eng. (2025) 112068.
[32] Y. Xie, W. Hutchison, H. Cui, J. Xue, Application of biochar to mitigate the autogenous shrinkage and improve mechanical performance of engineered geopolymer composites prepared with different ground granulated blast-furnace slag contents, Constr. Build. Mater. 486 (2025) 141973.
[33] Y. Xie, C. Wang, H. Wang, Y. Guo, H. Cui, J. Xue, Potential improvement in the mechanical performance and thermal resistance of geopolymer with appropriate microplastic incorporation: a sustainable solution for recycling and reusing microplastics, Waste Manag. 189 (2024) 137–147.
[34] P. Song, Y. Liu, L. Kong, Z. Tang, G. Sun, Research on design and optimization for compositions of ultra-high-performance geopolymer concrete, J. Build. Eng. 100 (2025) 111750.
[35] I. Eltantawi, M.N. Sheikh, M.N. Hadi, Design of a novel ternary blended self-compacting ultra-high-performance geopolymer concrete, Constr. Build. Mater. 451 (2024) 138819.
[36] Z. Ma, Y. Jiang, J. He, P. Shen, Q. Qin, Z. Gu, J. Li, C.S. Poon, Revealing the connection between carbonation regimes and early pozzolanic reactivity of recycled concrete powder: Impact of composition and microstructure, Cem. Concr. Res. 186 (2024) 107697.
[37] A. De Rossi, M. Ribeiro, J. Labrincha, R. Novais, D. Hotza, R. Moreira, Effect of the particle size range of construction and demolition waste on the fresh and hardened-state properties of fly ash-based geopolymer mortars with total replacement of sand, Process Saf. Environ. Prot. 129 (2019) 130–137.
[38] G. da Luz, P.J.P. Gleize, E.R. Batiston, F. Pelisser, Effect of pristine and functionalized carbon nanotubes on microstructural, rheological, and mechanical behaviors of metakaolin-based geopolymer, Cem. Concr. Compos. 104 (2019) 103332.
[39] ASTM C642, Standard Test Method for Density, Absorption, and Voids in Hardened Concrete, ASTM International (2021).
[40] ASTM C1698, Standard Test Method for Autogenous Strain of Cement Paste and Mortar, ASTM International (2019).
[41] ASTM C596, Standard Test Method for Drying Shrinkage of Mortar Containing Hydraulic Cement, ASTM International (2023).

[42] ASTM C109/109M, Standard Test Method for Compressive Strength of Hydraulic Cement Mortars (Using 50 mm [2 in.] Cube Specimens), ASTM International (2024).
[43] H. Yokota, K. Rokugo, N. Sakata, JSCE recommendations for design and construction of high performance fiber reinforced cement composite with multiple fine cracks, High. Perform. Fiber Reinf. Cem. Compos. 2 (2008) 761–770.
[44] D. Zhang, J. Yu, H. Wu, B. Jaworska, B.R. Ellis, V.C. Li, Discontinuous micro-fibers as intrinsic reinforcement for ductile Engineered Cementitious Composites (ECC), Composites Part B Engineering 184 (2020) 107741.
[45] Y. Bai, A. Arulrajah, S. Horpibulsuk, A. Zhou, Geopolymer stabilization of carbon-negative gasified olive stone biochar as a subgrade construction material, Constr. Build. Mater. 442 (2024) 137617.
[46] M. Whitaker, G.A. Heath, P. O'Donoughue, M. Vorum, Life cycle greenhouse gas emissions of coal-fired electricity generation: Systematic review and harmonization, J. Ind. Ecol. 16 (2012) S53–S72.
[47] S. Patel, A. Orlov, E. Ariyachandra, S. Peethamparan, Effect of flue gas temperature on NO2 adsorption by aged recycled concrete waste: DRIFTS, TGA and BET study, Chem. Eng. J. 420 (2021) 130413.
[48] F. Kaddah, E. Rozière, H. Ranaivomanana, O. Amiri, Complementary use of thermogravimetric analysis and oven to assess the composition and bound CO2 content of recycled concrete aggregates, Dev. Built Environ. 15 (2023) 100184.
[49] D. Chen, M. Chen, Y. Zhang, X. Yang, J. Zhang, Y. Zhao, Y. Wu, Development of an environmental foamed concrete incorporating recycled cement concrete powder with carbonation, Constr. Build. Mater. 422 (2024) 135833.
[50] J. Wu, Y. Ding, M. Guo, S. Guo, Fracture behaviour of modelled interfacial transition zone in recycled aggregate concrete prepared with carbonated aggregate, Constr. Build. Mater. 449 (2024) 138297.
[51] W. Dong, Q. Zhan, X. Zhang, Y. Su, J. Zhou, Study on accelerating activation of recycled hardened concrete powder based on microbial induced calcium precipitation, Constr. Build. Mater. 411 (2024) 134710.
[52] Y. Xie, Effects of biochar on the shrinkage and mechanical properties of sustainable engineered geopolymer composites: A comparative study between biochar sources, pyrolysis temperatures, and particle sizes, Clean. Mater. (2025) 100345.
[53] B. Yuan, Q. Yu, E. Dainese, H. Brouwers, Autogenous and drying shrinkage of sodium carbonate activated slag altered by limestone powder incorporation, Constr. Build. Mater. 153 (2017) 459–468.
[54] S. Yin, M. Liu, L. Shen, J. Zhu, The influence of superabsorbent polymers on the mechanical and shrinkage properties of engineered geopolymer composites, Constr. Build. Mater. 493 (2025) 143252.
[55] Y. Zheng, W. Guo, B. Jiang, N. Song, Y. Su, J. Zhang, Y. Zhang, J. Yu, B. Li, Understanding the role of superabsorbent polymers in engineered geopolymer composites, Constr. Build. Mater. 458 (2025) 139770.
[56] V. Revilla-Cuesta, L. Evangelista, J. de Brito, V. Ortega-López, J.M. Manso, Effect of the maturity of recycled aggregates on the mechanical properties and autogenous and drying shrinkage of high-performance concrete, Constr. Build. Mater. 299 (2021) 124001.
[57] Z. Li, Y. Chen, J.L. Provis, Ö. Cizer, G. Ye, Autogenous shrinkage of alkali-activated slag: A critical review, Cem. Concr. Res. 172 (2023) 107244.
[58] H. Zhang, J. Xiao, Y. Tang, Z. Duan, C.-s Poon, Long-term shrinkage and mechanical properties of fully recycled aggregate concrete: Testing and modelling, Cem. Concr. Compos. 130 (2022) 104527.
[59] Y. Xie, H. Wang, Y. Guo, C. Wang, H. Cui, J. Xue, Effects of microplastic contamination on the hydraulic, water retention, and desiccation crack properties of a natural clay exposed to leachate, J. Environ. Manag. 351 (2024) 119858.
[60] F. Li, Q. Chen, Y. Lu, Y. Zou, S. Li, Dry shrinkage and micro-structure of alkali-activated fly ash/slag pastes incorporated with silane coupling agent modified MWCNTs, Cem. Concr. Res. 175 (2024) 107382.
[61] B. Li, J. Wu, N. Song, Y. Zheng, Y. Lu, Y. Chi, Time-dependent drying shrinkage model for alkali-activated slag/fly ash-based concrete modified with multi-walled carbon nanotubes, J. Build. Eng. 111 (2025) 113082.
[62] H. Bian, L. Chai, Y. Liu, P. Duan, W. Shi, J. Chen, H. Zhang, Z. Ge, Prediction model for time-dependent drying shrinkage of recycled coarse and fine aggregate concrete based on internal relative humidity, Constr. Build. Mater. 439 (2024) 137426.
[63] N. Zhang, Q. Yang, D. Li, Y. Yu, X. Jiang, J. Xu, Autogenous and drying shrinkage properties of precast recycled aggregate concrete, Case Stud. Constr. Mater. 22 (2025) e04355.
[64] E.A. Ohemeng, S.O. Ekolu, H. Quainoo, D. Kruger, Model for predicting compressive strength and elastic modulus of recycled concrete made with treated coarse aggregate: Empirical approach, Constr. Build. Mater. 320 (2022) 126240.
[65] F. Li, Q. Chen, Y. Lu, Y. Zou, S. Li, Mitigating drying shrinkage and enhancing mechanical strength of fly ash-based geopolymer paste with functionalized MWCNTs grafted with silane coupling agent, Cem. Concr. Compos. 143 (2023) 105250.
[66] J. Bao, S. Li, Z. Yu, J. Xu, Y. Li, P. Zhang, Z. Si, S. Gao, Water transport in recycled aggregate concrete under sustained compressive loading: Experimental investigation and mesoscale numerical modelling, J. Build. Eng. 44 (2021) 103373.
[67] A. Noushini, A. Castel, J. Aldred, A. Rawal, Chloride diffusion resistance and chloride binding capacity of fly ash-based geopolymer concrete, Cem. Concr. Compos. 105 (2020) 103290.
[68] N.S.A. Júnior, J.S.A. Neto, H.A. Santana, M.S. Cilla, D.V. Ribeiro, Durability and service life analysis of metakaolin-based geopolymer concretes with respect to chloride penetration using chloride migration test and corrosion potential, Constr. Build. Mater. 287 (2021) 122970.
[69] T. Chen, Z. Yang, H. Liu, L. Li, L. Qin, X. Gao, Effect of biochar characteristics on freeze-thaw durability of biochar-cement composites, J. Build. Eng. 102 (2025) 111959.
[70] Z. Zhang, J. Yu, F. Qin, F. Sun, Thermal effect on mechanical properties of metakaolin-based engineered geopolymer composites (EGC), Case Stud. Constr. Mater. 18 (2023) e02150.
[71] F. Wang, J. Zhai, Y. Ding, T. Nishiwaki, J. Yu, V.C. Li, K. Yu, Design-driven approach for engineered geopolymer composite with recorded low fiber content, Composites Part B Engineering 287 (2024) 111834.
[72] Y. Jiang, B. Li, S. Liu, J. He, A.G. Hernandez, Role of recycled concrete powder as sand replacement in the properties of cement mortar, J. Clean. Prod. 371 (2022) 133424.
[73] S. Gupta, H.W. Kua, Carbonaceous micro-filler for cement: Effect of particle size and dosage of biochar on fresh and hardened properties of cement mortar, Sci. Total Environ. 662 (2019) 952–962.
[74] M. Liu, R. Hu, Y. Zhang, C. Wang, Z. Ma, Effect of ground concrete waste as green binder on the micro-macro properties of eco-friendly metakaolin-based geopolymer mortar, J. Build. Eng. 68 (2023) 106191.
[75] X. Wang, S. Dong, Z. Li, B. Han, J. Ou, Nanomechanical characteristics of interfacial transition zone in nano-engineered concrete, Engineering 17 (2022) 99–109.
[76] L. Lv, Y. Gan, B. Wen, L. Dai, J. Chen, L. Kan, Z. Zhang, Investigation of mechanical properties and microstructural evolution of ternary high-temperature resistant engineered geopolymer composite (EGC), Constr. Build. Mater. 487 (2025) 142082.
[77] L.-Y. Xu, J. Lao, L. Qian, D. Shi, J. Lan, T. Xie, D. Hou, B. Huang, Upcycling red mud into High-Strength High-Ductility Engineered Geopolymer Composites (EGC): Toward superior performance and sustainability, Compos. Part B Eng. (2025) 112713.
[78] P. Zhang, X. Han, J. Guo, S. Hu, High-temperature behavior of geopolymer mortar containing nano-silica, Constr. Build. Mater. 364 (2023) 129983.
[79] H. Bi, Z. Tang, F. Wang, L. Li, B. Mirzaev, K. Yu, L. Liu, Sustainable one-part engineered geopolymer composite with thermal insulation in coastal region: Utilizing red mud dual-function as precursor and activator, Case Stud. Constr. Mater. (2025) e04998.
[80] L. Kan, Y. Gan, L. Lv, L. Dai, W. Dai, Y. Lin, J. Li, Z. Zhang, Thermal impacts on eco-friendly ultra-lightweight high ductility geopolymer composites doped with low fiber volume, Constr. Build. Mater. 458 (2025) 139607.
[81] C.L. Chan, M. Zhang, Behaviour of strain hardening geopolymer composites at elevated temperatures, Cem. Concr. Compos. 132 (2022) 104634.
[82] Z. Zhang, J.-C. Liu, J. Li, F. Qin, J. Di, Micromechanics-based analysis of PVA–ECC after thermal exposure, Arch. Civ. Mech. Eng. 23 (3) (2023) 213.
[83] P. Zhang, Y. Sun, J. Wu, J. Hong, Z. Gao, Mechanical properties and microstructure of nano-modified geopolymer concrete containing hybrid fibers after exposure to elevated temperature, Constr. Build. Mater. 409 (2023) 134044.
[84] P. Zhang, B. Shi, X. Dai, C. Chen, C. Lai, A state-of-the-art review on the freeze–thaw resistance of sustainable geopolymer gel composites: mechanisms, determinants, and models, Gels 11 (7) (2025) 537.
[85] H. Nazarpour, M. Jamali, Mechanical and freezing cycles properties of geopolymer concrete with recycled aggregate, Struct. Concr. 21 (3) (2020) 1004–1012.
[86] F. Şahin, M. Uysal, O. Canpolat, Systematic evaluation of the aggregate types and properties on metakaolin based geopolymer composites, Constr. Build. Mater. 278 (2021) 122414.
[87] A.İ. Uğurlu, M.B. Karakoc, A. Özcan, Effect of binder content and recycled concrete aggregate on freeze-thaw and sulfate resistance of GGBFS based geopolymer concretes, Constr. Build. Mater. 301 (2021) 124246.
[88] F. Li, D. Chen, Y. Lu, H. Zhang, S. Li, Influence of mixed fibers on fly ash based geopolymer resistance against freeze-thaw cycles, J. NonCryst. Solids 584 (2022) 121517.